Article

The International Journal of Robotics Research
2014, Vol 33(1) 48–68

DOI: 10.1177/0278364912473169
ijr.sagepub.com

Quasi-static manipulation of a Kirchhoff elastic rod based on a geometric analysis of equilibrium configurations

Timothy Bretl[1] and Zoe McCarthy[2]

Abstract

Consider a thin, flexible wire of fixed length that is held at each end by a robotic gripper. Any curve traced by this wire when in static equilibrium is a local solution to a geometric optimal control problem, with boundary conditions that vary with the position and orientation of each gripper. We prove that the set of all local solutions to this problem over all possible boundary conditions is a smooth manifold of finite dimension that can be parameterized by a single chart. We show that this chart makes it easy to implement a sampling-based algorithm for quasi-static manipulation planning. We characterize the performance of such an algorithm with experiments in simulation.

Keywords

Manipulation planning, manipulation, path planning for manipulators, manipulation, mechanics, design and control

1. Introduction

Figure 1 shows a thin, flexible wire of fixed length that is held at each end by a robotic gripper. Our basic problem of interest is to find a path of each gripper that causes the wire to move between start and goal configurations while remaining in static equilibrium and avoiding self-collision. As will become clear, it is useful to think about this problem equivalently as finding a path *of the wire* through its set of equilibrium configurations (i.e. the set of all configurations that would be in equilibrium if both ends of the wire were held fixed).

There are two reasons why this problem seems hard to solve. First, the configuration space of the wire has infinite dimension. Elements of this space are framed curves, i.e. continuous maps $q\colon [0,1] \to SE(3)$, the shape of which in general must be approximated. Second, a countable number of configurations may be in static equilibrium for given placements of each gripper, none of which can be computed in closed form. For these two reasons, the literature on manipulation planning suggests exploring the set of equilibrium configurations indirectly, by sampling displacements of each gripper and using numerical simulation to approximate their effect on the wire. This approach was developed in the seminal work of Lamiraux and Kavraki (2001) and was applied by Moll and Kavraki (2006) to manipulation of elastic "deformable linear objects" like the flexible wire we consider here.

Our contribution in this paper is to show that the set of equilibrium configurations for the wire is a smooth manifold of finite dimension that can be parameterized by a single (global) coordinate chart. We model the wire as a Kirchhoff elastic rod (Biggs et al., 2007). The framed curve traced by this rod in static equilibrium can be described as a local solution to a geometric optimal control problem, with boundary conditions that vary with the position and orientation of each gripper (Walsh et al., 1994; Biggs et al., 2007). Coordinates for the set of *all* local solutions over *all* boundary conditions are provided by the initial value of co-states that arise in necessary and sufficient conditions for optimality. These coordinates describe all possible configurations of the elastic rod that can be achieved by quasi-static manipulation, and make manipulation planning—the seemingly "hard problem" described above—very easy to solve. We will provide both analytical and empirical results to justify this claim in the context of a sampling-based planning algorithm. For now, we note that the computations ultimately required by our approach are trivial to implement.

A variety of applications motivate our work: knot tying and surgical suturing (Hopcroft et al., 1991; Takamatsu et al., 2006; Wakamatsu et al., 2006; Saha and Isto, 2007; Bell and Balkcom, 2008), cable routing (Inoue and

[1]Department of Aerospace Engineering, University of Illinois at Urbana-Champaign, USA
[2]Electrical and Computer Engineering, University of Illinois at Urbana-Champaign, USA

Corresponding author:
Timothy Bretl, Department of Aerospace Engineering, University of Illinois at Urbana-Champaign, 306 Talbot Lab, MC-236 104 South Wright Street, Urbana, IL 61801, USA.
Email: tbretl@illinois.edu

Inaba, 1985), folding clothes (van den Berg et al., 2011; Yamakawa et al., 2011), compliant parts handling (Lin et al., 2000; Gopalakrishnan and Goldberg, 2005) and assembly (Asano et al., 2010), surgical retraction of tissue (Jansen et al., 2009), protein folding (Amato and Song, 2002), haptic exploration with "whisker" sensors that are modeled as elastic rods (Clements and Rahn, 2006; Solomon and Hartmann, 2010), etc. We are also motivated by the link, pointed out by Tanner (2006), between manipulation of deformable objects and control of hyper-redundant (Chirikjian and Burdick, 1995) and continuum (Rucker et al., 2010; Webster and Jones, 2010) robots. However, we acknowledge that our work in this paper is theoretical and that much remains to be done before any of it can be applied in practice.

Section 2 gives a brief overview of prior approaches to quasi-static manipulation of "deformable linear objects" like the elastic rod. Section 3 provides an introduction to the key ideas by consideration of a simpler example, namely an elastic rod that is confined to a planar workspace. Section 4 establishes our theoretical framework. The two key parts of this framework are optimal control on manifolds and Lie–Poisson reduction. We derive coordinate formulae for necessary and sufficient conditions—in the former case these formulae are well known, but in the latter case they are not. Section 5 shows how our framework applies to the Kirchhoff elastic rod. We prove that the set of all equilibrium configurations for this rod is a smooth manifold of finite dimension that can be parameterized by a single chart. Section 6 explains why this result makes the problem of manipulation planning easy to solve. Section 7 identifies several limitations of our approach and suggests ways these limitations might be addressed.

A preliminary version of this paper has appeared at a conference (Bretl and McCarthy, 2012). Several extensions are provided here. The discussion of related work in Section 2 and the consideration of a planar elastic rod in Section 3 are both new, as are the physical interpretation of the coordinate chart we derive (Section 5.4), the precise definition of "straight-line paths" both in this chart and in the space of boundary conditions (Section 5.5), the summary of computations required by our approach, and the empirical results in simulation that we use to justify our choice of local connection strategy (Section 6.2). In addition, we provide a more direct proof of Lemma 4, which is the basis for our main result in Section 5.2. Our ideas in this paper also follow from, but significantly extend, earlier work on a simpler model (McCarthy and Bretl, 2012).

2. Related work

There are two main approaches to manipulation planning for "deformable linear objects" like the elastic rod we consider here, one that relies primarily on numerical simulation and another that uses task-based decomposition.

The first approach is exemplified by Moll and Kavraki (2006), who provide a sampling-based planning algorithm for quasi-static manipulation of an inextensible elastic rod—as might be used to model flexible wire or surgical thread—by robotic grippers in a three-dimensional (3D) workspace. Any framed curve traced by this rod when in static equilibrium is one that locally minimizes total elastic energy, defined as the integral of squared curvature plus squared torsion along the rod's entire length.[1] The algorithm proceeds by sampling placements of each gripper and by using numerical methods to find minimal-energy curves that satisfy these boundary conditions. It measures the distance between curves by the integral of the sum-squared difference in curvature and torsion, and connects nearby curves by spherical interpolation of gripper placement (i.e. by a local path in the space of boundary conditions), again using numerical methods to find the resulting path of the rod. The choice of numerical methods clearly has a significant impact on the performance of this approach. Moll and Kavraki (2006) approximate minimal-energy curves by recursive subdivision. Many other methods have been proposed (finite element, finite difference, etc.) that we will not mention here, since they are used for planning in much the same way. The current state-of-the-art is perhaps the discrete geometric model of Bergou et al. (2008), which has recently found application in robotics (Javdani et al., 2011).

The second approach is exemplified by the work of Wakamatsu et al. (2006) and of Saha and Isto (2007) on knot tying with rope. Knot tying is an example of a manipulation task in which the goal is topological rather than geometric. It does not matter exactly what curve is traced by the rope, only that this curve has the correct sequence of crossings. Motion primitives can be designed to ensure that crossing operations are realizable by robotic grippers—Wakamatsu et al. (2006) use primitives that rely on the rope being placed on a table and immobilized by gravity, while Saha and Isto (2007) use primitives that rely on fixtures, which they refer to as "needles" by analogy to knitting. This approach has been generalized to folding paper by Balkcom and Mason (2008) and to folding clothes by van den Berg et al. (2011). "Crossings" are replaced by "folds," again realized either by relying on fixtures or on immobilization by gravity.

Like the first approach, we consider a geometric goal in this paper and model equilibrium configurations as local minima of total elastic energy. However, instead of relying on numerical simulation, we will derive coordinates that explicitly describe the set of all possible equilibrium configurations for our object of interest, a Kirchhoff elastic rod. This result will allow us to plan a path *of the rod* through its set of equilibrium configurations—like the second approach—rather than plan indirectly by sampling placements of each gripper.

We have been strongly influenced by prior analysis of the Kirchhoff elastic rod using calculus of variations and optimal control. This analysis has been done both from a

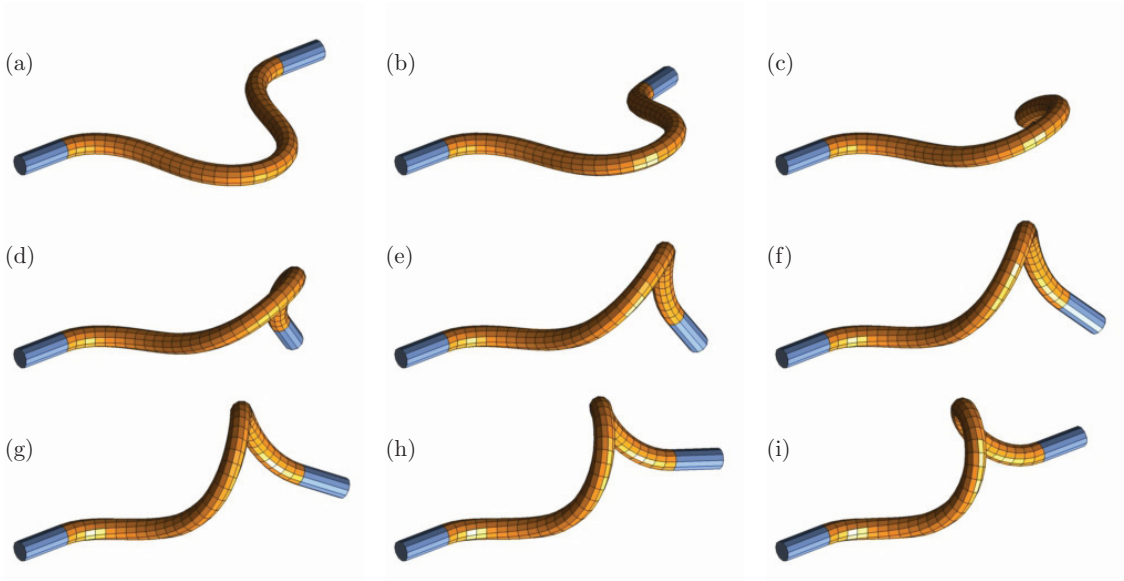

Fig. 1. Quasi-static manipulation of an elastic rod (orange) by robotic grippers (blue). Notice that the grippers begin (fa) and end (i) in the same position and orientation. This motion corresponds to a single straight-line path in the global coordinate chart we derive in this paper.

Lagrangian (Langer and Singer, 1984, 1996) and a Hamiltonian (Walsh et al., 1994; Jurdjevic, 2005; Biggs et al., 2007) perspective. It has led in some cases to global descriptions of extremal solutions—often called "solution manifolds"—similar to what we derive in this paper. For example, Ivey and Singer (1999) show that closed and quasi-periodic extremals of uniform, isotropic, linearly elastic rods are parameterized by a two-dimensional (2D) disc. Similarly, Neukirch and Henderson (2002) classify extremals of elastic rods with clamped boundary conditions and apply numerical continuation to explicitly compute the set of all such extremals (Henderson and Neukirch, 2004). Recent work in particular gives a more or less complete picture of planar elastic rods (Sachkov, 2008a, 2008b) and builds on the same basic theory—from Agrachev and Sachkov (2004)—that we use in this paper. We also note the study of conjugate points in elastic filament models of DNA by Hoffman (2004). The sufficient conditions for optimality that we derive in the following two sections essentially rely on the non-existence of conjugate points. None of this work has been applied yet to manipulation planning—Camarillo et al. (2008) and Rucker et al. (2010) are closest to making this link, in the context of continuum robots (e.g. tendon-driven or concentric-tube).

In this discussion, we have omitted previous work that is not directly related either to analysis or manipulation of a Kirchhoff elastic rod. Our results may nonetheless have some relevance to this other work (e.g. on fair curves and minimal-energy splines in computer graphics) that it might be useful to explore. Readers may refer to the survey provided by Moll and Kavraki (2006) or to the text of Antman (2005) for a broader overview.

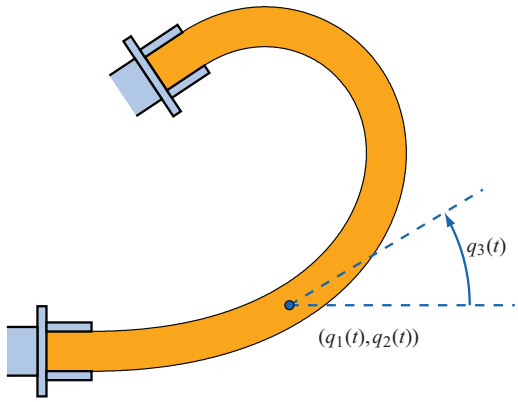

Fig. 2. A planar elastic rod in static equilibrium, held at each end by a robotic gripper.

3. Planar example

In this section, we briefly consider the manipulation of an elastic rod that is confined to a planar workspace. Our discussion is relatively informal and is meant to introduce some basic concepts that we will develop throughout the remainder of this paper.

3.1. Static equilibrium as optimal control

We call the object in Figure 2 a *planar elastic rod*. Assuming it is thin, inextensible, and unit length, we describe the shape of this rod by a continuous map $q\colon [0,1] \to \mathbb{R}^3$. The elements $q_1(t)$ and $q_2(t)$ are the "x" and "y" coordinates of the curve traced by the rod at any point $t \in [0,1]$, and the

element $q_3(t)$ is the tangent angle to this curve. We require the map q to satisfy

$$\begin{aligned} \dot{q}_1 &= \cos q_3 \\ \dot{q}_2 &= \sin q_3 \\ \dot{q}_3 &= u \end{aligned} \tag{1}$$

for some $u\colon [0,1] \to \mathbb{R}$, which can be interpreted as strain (in bending). We refer to q and u together as (q,u). We assume that the base of the rod is held fixed at the origin, so that $q(0) = 0$. The other end is held by a robotic gripper, which we assume can impose arbitrary $q(1) \in \mathbb{R}^3$. For fixed $q(1)$, the rod will remain motionless only if its shape locally minimizes total elastic energy. In particular, we say that (q,u) is in *static equilibrium* if it is a local optimum of the deterministic, continuous-time, optimal control problem

$$\begin{aligned} \underset{q,u}{\text{minimize}} \quad & \frac{1}{2}\int_0^1 u^2 \mathrm{d}t \\ \text{subject to} \quad & \dot{q} = \begin{bmatrix} \cos q_3 \\ \sin q_3 \\ u \end{bmatrix} \\ & q(0) = 0 \\ & q(1) = b \end{aligned} \tag{2}$$

for some $b \in \mathbb{R}^3$. The cost function in equation (2) is a commonly used, first-order approximation to elastic energy that is valid under the assumption of small deformations. This assumption requires only that the strain $u(t)$ stays small, not that changes in the configuration (q,u) are small. In particular, the configuration shown in Figure 2 exhibits "small deformations" (as do the configurations in Figure 1 and, indeed, in all of the examples considered in this paper). We also note that although equilibrium configurations (q,u) are local optima of equation (2), there is nothing "local" about our model. Every possible equilibrium configuration is a local optimum of equation (2) for some choice of b.

3.2. Quasi-static manipulation

Small changes $b + \delta b$ in gripper placement will, in general, give rise to small changes $(q + \delta q, u + \delta u)$ in a local optimum of equation (2), i.e. in an equilibrium configuration of the planar elastic rod. The problem of *quasi-static manipulation planning* is to find a continuous map $\beta\colon [0,1] \to \mathbb{R}^3$ so that as s increases continuously from 0 to 1, there is a local optimum of equation (2) with $b = \beta(s)$ that changes continuously from $(q_{\text{start}}, u_{\text{start}})$ to $(q_{\text{goal}}, u_{\text{goal}})$.

An immediate challenge in searching for β is that the gripper placement b does not uniquely define the configuration (q,u) of the rod. In general, equation (2) has many local optima for fixed b (e.g. see Figure 3), none of which can be computed in closed form. A similar challenge arises in path planning for pick-and-place motions of an n-joint robot arm, where there are (in general) many inverse kinematic solutions for a given placement of the end-effector. There, we can avoid reasoning about the multiplicity of inverse kinematic solutions by planning in the joint space (e.g. $S^1 \times \cdots^{n} \times S^1$) rather than in the task space (e.g. $SE(3)$). We would like to apply this same approach to quasi-static manipulation, planning a path *of the rod* rather than of the gripper. However, it is not obvious how to describe the set of all equilibrium configurations (i.e. the set of *all* local optima of equation (2) over *all* possible $b \in \mathbb{R}^3$), which is the natural analog of "joint space" in this context. We show how to do this in the following section.

3.3. Analysis of equilibrium configurations

Considerable insight can be obtained by applying the maximum principle of Pontryagin et al. (1962) to the optimal control problem equation (2). If

$$(q,u) : [0,1] \to \mathbb{R}^3 \times \mathbb{R}$$

is a local optimum of equation (2), then the maximum principle tells us that there must exist a *co-state trajectory*

$$p\colon [0,1] \to \mathbb{R}^3$$

and a constant $k \geq 0$, not both zero, that satisfy

$$\begin{aligned} \dot{q} &= \nabla_p H(p,q,k,u)^T \\ \dot{p} &= -\nabla_q H(p,q,k,u)^T \end{aligned} \tag{3}$$

and

$$H\left(p(t), q(t), k, u(t)\right) = \max_v H\left(p(t), q(t), k, v\right) \tag{4}$$

for all $t \in [0,1]$, where

$$H(p,q,k,u) = p_1 \cos q_3 + p_2 \sin q_3 + p_3 u - k\frac{1}{2}u^2$$

is the *Hamiltonian function* associated with equation (2).

When applying these necessary conditions, we often distinguish between the *abnormal case* in which $k = 0$, and the *normal case* in which $k > 0$, where as usual we may simply assume that $k = 1$ (see, for example, Souéres and Boissonnat (1998)). Taking the abnormal case first, the conditions in equations (3) and (4) require that

$$\begin{aligned} \dot{q}_1 &= \cos q_3 & \dot{p}_1 &= 0 \\ \dot{q}_2 &= \sin q_3 & \dot{p}_2 &= 0 \\ \dot{q}_3 &= u & \dot{p}_3 &= p_1 \sin q_3 - p_2 \cos q_3 \end{aligned} \tag{5}$$

and

$$0 = p_3,$$

respectively. Since p_1, p_2, and

$$p_1 \sin q_3 - p_2 \cos q_3$$

are evidently all constant, it must be the case that q_3 is also constant. We conclude that (q,u) is "abnormal" if and only if $u(t) = 0$ for all $t \in [0,1]$, i.e. if and only if the rod

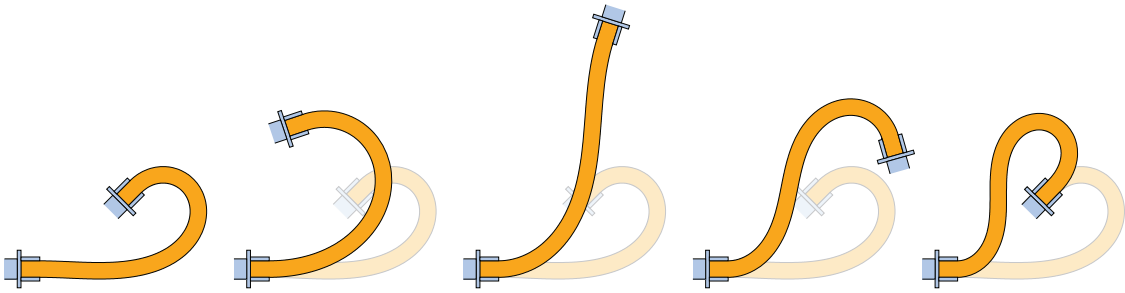

Fig. 3. Quasi-static manipulation of a planar elastic rod. Notice that the grippers begin and end in the same position and orientation–gripper placement does not uniquely define the configuration of the rod.

is straight. Turning now to the normal case, equation (3) requires equation (5) just as before, while equation (4) now requires that

$$u = p_3. \tag{6}$$

From equations (5) and (6), we see that "normal" (q, u) and p are completely defined by $p(0)$, the choice of initial co-state. It is also easy to verify that

$$u(t) = 0 \text{ for all } t \in [0,1] \quad \Longleftrightarrow \quad p_2(0) = p_3(0) = 0,$$

so every abnormal (q, u) is also normal. As a consequence, every possible equilibrium configuration of the planar elastic rod can be generated by an appropriate choice of $p(0) \in \mathbb{R}^3$. In particular, the set of *all* equilibrium configurations—analogous to the "joint space" for an n-joint robot arm—is apparently a subset of $\mathbb{R}^3$. This result is already somewhat remarkable, given that arbitrary configurations (q, u) live in a space of infinite dimension.

3.4. Physical interpretation of the co-state trajectory

The co-state trajectory $p\colon [0,1] \to \mathbb{R}^3$ that is produced by application of the maximum principle has a physical interpretation. To provide this interpretation, we begin by assuming that $p(t)$ describes the force and torque acting on the rod at $t \in [0,1]$, and proceed to check if this assumption allows us to reconstruct the governing equations equation (5) and equation (6). In particular, consider a small piece of the planar elastic rod, as shown in Figure 4(a). In static equilibrium, a force and torque balance requires that

$$\begin{aligned}
p_1(t+\Delta t) - p_1(t) &= 0 \\
p_2(t+\Delta t) - p_2(t) &= 0 \\
p_3(t+\Delta t) - p_3(t) &= p_1(t+\Delta t)\,(q_2(t+\Delta t) - q_2(t)) \\
&\quad - p_2(t+\Delta t)\,(q_1(t+\Delta t) - q_1(t)).
\end{aligned}$$

In the limit as $\Delta t \to 0$, we recover

$$\begin{aligned}
\dot{p}_1 &= 0 \\
\dot{p}_2 &= 0 \\
\dot{p}_3 &= p_1\dot{q}_2 - p_2\dot{q}_1 = p_1 \sin q_3 - p_2 \cos q_3,
\end{aligned} \tag{7}$$

exactly as in equation (5). Equation (6) follows immediately from the linear relationship between stress and strain. We conclude that $p(t)$ does indeed describe force and torque, and specifically that every equilibrium configuration is completely defined by the force and torque at the base of the rod (i.e. by $p(0)$). It is even possible to show that (q, u) is abnormal if and only if $p(0)$ is indeterminate, a result that will be useful to us in characterizing degeneracies of the mapping from $b + \delta b$ to $(q + \delta q, u + \delta u)$.

Before proceeding, we consider the same force and torque balance in a local reference frame, as in Figure 4(b). Define $\mu\colon [0,1] \to \mathbb{R}^3$ as

$$\begin{bmatrix} \mu_1(t) \\ \mu_2(t) \\ \mu_3(t) \end{bmatrix} = \begin{bmatrix} \cos q_3(t) & \sin q_3(t) & 0 \\ -\sin q_3(t) & \cos q_3(t) & 0 \\ 0 & 0 & 1 \end{bmatrix} \begin{bmatrix} p_1(t) \\ p_2(t) \\ p_3(t) \end{bmatrix}$$

for all $t \in [0,1]$. Either by applying this transform to equation (7) or by taking a force and torque balance, we find that

$$\begin{aligned}
\dot{\mu}_1 &= \mu_2\mu_3 \\
\dot{\mu}_2 &= -\mu_1\mu_3 \\
\dot{\mu}_3 &= -\mu_2,
\end{aligned} \tag{8}$$

where $u = \mu_3$. Equations (7) and (8) are equivalent—any equilibrium configuration can be generated *either* by specifying $p(0)$ or by specifying $\mu(0)$. However, it is interesting to note that equation (8)—unlike equation (7)—has no dependence on q. This sort of "reduction" will become very important as we generalize our approach to a geometric setting.

Finally, notice that the signed curvature of the curve $(q_1, q_2) : [0,1] \to \mathbb{R}^2$ that is traced by the planar elastic rod is given by $\kappa = u = \mu_3$. It is easy to verify that

$$2\ddot{\kappa} + \kappa^3 = \lambda\kappa \tag{9}$$

and equation (8) are equivalent, where

$$\lambda = \mu_3(0)^2 + 2\mu_1(0)$$

is a constant of integration. In this way, we recover the variational constraint in equation (9) that would have been produced by analysis of equation (2) from a Lagrangian perspective (as in Langer and Singer (1984, 1996)).

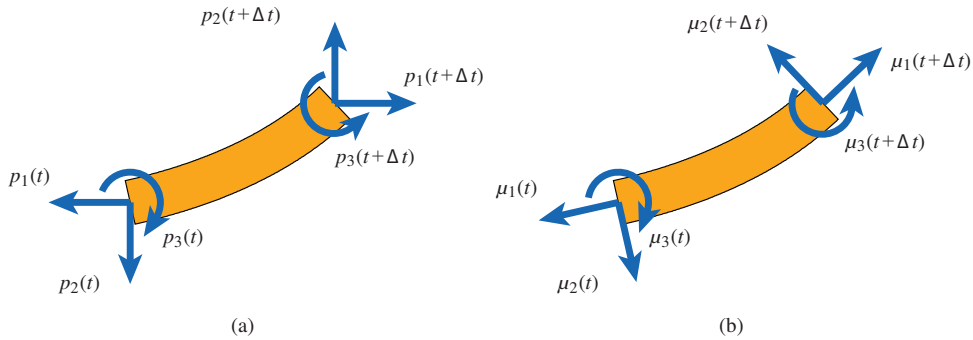

Fig. 4. Forces and torques applied to a piece of the planar elastic rod (a) in a global reference frame and (b) in a local reference frame, providing a physical interpretation of the co-state trajectory.

3.5. Outline

In the rest of this paper, we make precise the ideas discussed above and generalize them to enable quasi-static manipulation of an elastic rod in a 3D workspace. A key difference in what follows is that the rod's shape will be described by $q\colon [0,1] \to SE(3)$ instead of $q\colon [0,1] \to \mathbb{R}^3$, and consequently that equation (2) will become a problem of optimal control on manifolds. To obtain the necessary conditions for optimality that are analogous to what appeared in Section 3.3, we will be forced on rely on a geometric statement of Pontryagin's maximum principle. We provide these necessary conditions—as well as sufficient conditions, which were completely ignored in the above discussion and which are considerably more involved—in Section refsec:theory. We apply them to study the mechanics of the elastic rod in Section 5, and to study manipulation of this rod in Section 6.

4. Theoretical framework

We will see in Section 5 that the framed curve traced by an elastic rod in static equilibrium is a local solution to a geometric optimal control problem. Here, we provide the framework to characterize this solution. This framework essentially relies on a geometric statement of Pontryagin's maximum principle (Pontryagin et al., 1962). Section 4.1 reviews smooth manifolds and is included to fix notation. Section 4.2 states the necessary and sufficient conditions for optimality on manifolds in a form that is useful for us. Section 4.3 derives coordinate formulae to compute these necessary and sufficient conditions. Most of these results are a translation of Agrachev and Sachkov (2004) in a style more consistent with Marsden and Ratiu (1999) and Lee (2003). We conclude with coordinate formulae to test sufficiency for left-invariant systems on Lie groups (Theorem 4), an important result that is not in Agrachev and Sachkov (2004) and that is hard to find elsewhere.

4.1. Smooth manifolds

In this section, we review some basic facts about smooth manifolds. We do so mainly to establish notation for what follows.

Let M be a smooth manifold. The space of all smooth real-valued functions on M is $C^\infty(M)$. The space of all smooth vector fields on M is $\mathfrak{X}(M)$. The action of a tangent vector $v \in T_mM$ on a function $f \in C^\infty(M)$ is $v \cdot f$. The action of a tangent covector $w \in T_m^*M$ on a tangent vector $v \in T_mM$ is $\langle w, v\rangle$. The action of a vector field $X \in \mathfrak{X}(M)$ on a function $f \in C^\infty(M)$ produces the function $X[f] \in C^\infty(M)$ that satisfies

$$X[f](m) = X(m) \cdot f$$

for all $m \in M$. The Jacobi–Lie bracket of vector fields $X, Y \in \mathfrak{X}(M)$ is the vector field $[X,Y] \in \mathfrak{X}(M)$ that satisfies

$$[X,Y][f] = X[Y[f]] - Y[X[f]]$$

for all $f \in C^\infty(M)$. If $F\colon M \to N$ is a smooth map between smooth manifolds M and N, then the pushforward of F at $m \in M$ is the linear map $T_mF\colon T_mM \to T_{F(m)}N$ that satisfies

$$T_mF(v) \cdot f = v \cdot (f \circ F)$$

for all $v \in T_mM$ and $f \in C^\infty(N)$. The pullback of F at $m \in M$ is the dual map $T_m^*F\colon T_{F(m)}^*N \to T_m^*M$ that satisfies

$$\left\langle T_m^*F(w), v\right\rangle = \langle w, T_mF(v)\rangle$$

for all $v \in T_mM$ and $w \in T_{F(m)}^*N$. We say F is degenerate at $m \in M$ if there exists non-zero $v \in T_mM$ such that $T_mF(v) = 0$. It is equivalent that the Jacobian matrix of any coordinate representation of F at m has zero determinant. The Poisson bracket generated by the canonical symplectic form on T^*M is

$$\{\cdot,\cdot\}\colon C^\infty(T^*M) \times C^\infty(T^*M) \to C^\infty(T^*M).$$

The co-tangent bundle T^*M together with the bracket $\{\cdot,\cdot\}$ is a Poisson manifold. The Hamiltonian vector field of $H \in C^\infty(T^*M)$ is the unique vector field $X_H \in \mathfrak{X}(T^*M)$ that satisfies

$$X_H[K] = \{K, H\}$$

for all $K \in C^\infty(T^*M)$. It is equivalent to say that H is a Hamiltonian function for the vector field X_H. We use this same notation when H (hence, X_H) is time-varying. Finally, we use $\pi : T^*M \to M$ to denote the projection map satisfying $\pi(w,m) = m$ for all $w \in T_m^*M$.

4.2. Optimal control on manifolds

In this section, we state the necessary and sufficient conditions for optimal control problems on smooth manifolds. These conditions are analogous to what is provided by Pontryagin's maximum principle, which is usually applied to optimal control problems on Euclidean space.

Let $U \subset \mathbb{R}^m$ for some $m > 0$. Assume $g\colon M \times U \to \mathbb{R}$ and $f\colon M \times U \to TM$ are smooth maps. Consider the optimal control problem

$$\begin{aligned} \underset{q,u}{\text{minimize}} \quad & \int_0^1 g\left(q(t), u(t)\right) \mathrm{d}t \\ \text{subject to} \quad & \dot{q}(t) = f\left(q(t), u(t)\right) \text{ for all } t \in [0,1] \\ & q(0) = q_0, \qquad q(1) = q_1, \end{aligned} \tag{10}$$

where $q_0, q_1 \in M$ and $(q,u)\colon [0,1] \to M \times U$. Define the parameterized Hamiltonian function $\widehat{H}\colon T^*M \times \mathbb{R} \times U \to \mathbb{R}$ by

$$\widehat{H}(p,q,k,u) = \langle p, f(q,u)\rangle - kg(q,u),$$

where $p \in T_q^\star M$. The following theorem is a geometric statement of Pontryagin's maximum principle (Pontryagin et al., 1962):

Theorem 1 (Necessary conditions)**.** *Suppose* $(q_{\text{opt}}, u_{\text{opt}})\colon [0,1] \to M \times U$ *is a local optimum of equation* (10)*. Then, there exists* $k \geq 0$ *and an integral curve* $(p,q)\colon [0,1] \to T^*M$ *of the time-varying Hamiltonian vector field* X_H*, where* $H\colon T^*M \times \mathbb{R} \to \mathbb{R}$ *is given by* $H(p,q,t) = \widehat{H}(p,q,k,u_{\text{opt}}(t))$*, that satisfies* $q(t) = q_{\text{opt}}(t)$ *and*

$$H(p(t), q(t), t) = \max_{u \in U} \widehat{H}(p(t), q(t), k, u) \tag{11}$$

for all $t \in [0,1]$*. Furthermore, if* $k = 0$*, then* $p(t) \neq 0$ *for all* $t \in [0,1]$*.*

Proof. See Theorem 12.10 of Agrachev and Sachkov (2004). □

We call the integral curve (p,q) in Theorem 1 an abnormal extremal when $k = 0$ and a normal extremal otherwise. As usual, when $k \neq 0$ we may simply assume $k = 1$. We call (q,u) abnormal if it is the projection of an abnormal extremal. We call (q,u) normal if it is the projection of a normal extremal and it is not abnormal.

Theorem 2 (Sufficient conditions)**.** *Suppose* $(p,q)\colon [0,1] \to T^*M$ *is a normal extremal of equation* (10)*. Define* $H \in C^\infty(T^*M)$ *by*

$$H(p,q) = \max_{u \in U} \widehat{H}(p,q,1,u), \tag{12}$$

assuming the maximum exists and $\partial^2 \widehat{H}/\partial u^2 < 0$*. Define* $u\colon [0,1] \to U$ *so* $u(t)$ *is the unique maximizer of equation* (12) *at* $(p(t), q(t))$*. Assume that* X_H *is complete and that there exists no other integral curve* (p', q') *of* X_H *satisfying* $q(t) = q'(t)$ *for all* $t \in [0,1]$*. Let* $\varphi\colon \mathbb{R} \times T^*M \to T^*M$ *be the flow of* X_H *and define the endpoint map* $\phi_t\colon T^*_{q(0)}M \to M$ *by* $\phi_t(w) = \pi \circ \varphi(t, w, q(0))$*. Then,* (q,u) *is a local optimum of equation* (10) *if and only if there exists no* $t \in (0,1]$ *for which* ϕ_t *is degenerate at* $p(0)$*.*

Proof. See Theorem 21.8 of Agrachev and Sachkov (2004). □

4.3. Lie–Poisson reduction

The necessary and sufficient conditions provided by Theorems 1 and 2 are, in principle, all we need to characterize solutions to optimal control problems on manifolds. However, it is not apparent yet how to compute anything—in particular, how to compute integral curves (p,q) or to establish non-degeneracy of the endpoint map ϕ_t. In this section, we apply the Lie–Poisson reduction to provide coordinate formulae for computation in the specific case where the manifold is a Lie Group and the Hamiltonian function is left-invariant. As we will see in Section 5, this case is satisfied by a Kirchhoff elastic rod.

First, we establish some additional notation. Let G be a Lie group with identity element $e \in G$. Let $\mathfrak{g} = T_eG$ and $\mathfrak{g}^* = T_e^*G$. For any $q \in G$, define the left translation map $L_q\colon G \to G$ by

$$L_q(r) = qr$$

for all $r \in G$. A function $H \in C^\infty(T^*G)$ is left-invariant if

$$H\left(T_r^* L_q(w), r\right) = H(w,s)$$

for all $w \in T_s^*G$ and $q, r, s \in G$ satisfying $s = L_q(r)$. For any $\zeta \in \mathfrak{g}$, let X_ζ be the vector field that satisfies

$$X_\zeta(q) = T_e L_q(\zeta)$$

for all $q \in G$. Define the Lie bracket $[\cdot,\cdot]\colon \mathfrak{g} \times \mathfrak{g} \to \mathfrak{g}$ by

$$[\zeta, \eta] = \left[X_\zeta, X_\eta\right](e)$$

for all $\zeta, \eta \in \mathfrak{g}$. For any $\zeta \in \mathfrak{g}$, the adjoint operator $\mathrm{ad}_\zeta\colon \mathfrak{g} \to \mathfrak{g}$ satisfies

$$\mathrm{ad}_\zeta(\eta) = [\zeta, \eta]$$

and the co-adjoint operator $\mathrm{ad}_\zeta^*\colon \mathfrak{g}^* \to \mathfrak{g}^*$ satisfies

$$\left\langle \mathrm{ad}_\zeta^*(\mu), \eta \right\rangle = \left\langle \mu, \mathrm{ad}_\zeta\, \eta \right\rangle$$

for all $\eta \in \mathfrak{g}$ and $\mu \in \mathfrak{g}^*$. The functional derivative of $h \in C^\infty(\mathfrak{g}^*)$ at $\mu \in \mathfrak{g}^*$ is the unique element $\delta h/\delta\mu$ of $\mathfrak{g}$ that satisfies

$$\lim_{s \to 0} \frac{h(\mu + s\delta\mu) - h(\mu)}{s} = \left\langle \delta\mu, \frac{\delta h}{\delta \mu} \right\rangle$$

for all $\delta\mu \in \mathfrak{g}^*$.

Next, we revisit our statement of necessary conditions for the optimal control problem equation (10) in the case where $M = G$ and where the Hamiltonian H is left-invariant. Theorem 1 implies the existence of a particular integral curve

(p, q) in the cotangent bundle T^*G. The following theorem implies the existence of a corresponding integral curve μ in the dual Lie algebra $\mathfrak{g}^*$. This result is important because $\mathfrak{g}^*$ is a vector space and so μ can be readily computed by solving a system of ordinary differential equations, as we will see in Theorem 4 (to follow).

Theorem 3 (Reduction of necessary conditions)**.** *Suppose the time-varying Hamiltonian function $H\colon T^*G \times [0,1] \to \mathbb{R}$ is both smooth and left-invariant for all $t \in [0,1]$. Denote the restriction of H to $\mathfrak{g}^*$ by $h = H|_{\mathfrak{g}^* \times [0,1]}$. Given $p_0 \in T^*_{q_0}G$, let $\mu\colon [0,1] \to \mathfrak{g}^*$ be the solution of*

$$\dot{\mu} = \mathrm{ad}^*_{\delta h/\delta \mu}(\mu) \tag{13}$$

with initial condition $\mu(0) = T^*_e L_{q_0}(p_0)$. The integral curve $(p, q)\colon [0,1] \to T^*G$ of X_H with initial condition $p(0) = p_0$ satisfies

$$p(t) = T^*_{q(t)} L_{q(t)^{-1}}(\mu(t))$$

for all $t \in [0,1]$, where q is the solution of

$$\dot{q} = X_{\delta h/\delta \mu}(q)$$

with initial condition $q(0) = q_0$.

Proof. See Theorem 13.4.4 of Marsden and Ratiu (1999). □

In what follows, it will be convenient for us to introduce coordinates on $\mathfrak{g}$ and $\mathfrak{g}^*$. Let $\{X_1, \ldots, X_n\}$ be a basis for $\mathfrak{g}$ and let $\{P_1, \ldots, P_n\}$ be the dual basis for $\mathfrak{g}^*$ that satisfies

$$\langle P_i, X_j \rangle = \delta_{ij},$$

for $i, j \in \{1, \ldots, n\}$, where δ_{ij} is the Kronecker delta. We write ζ_i to denote the ith component of $\zeta \in \mathfrak{g}$ with respect to this basis, and so forth. Define the structure constants $C^k_{ij} \in \mathbb{R}$ associated with our choice of basis by

$$[X_i, X_j] = \sum_{k=1}^{n} C^k_{ij} X_k \tag{14}$$

for $i, j \in \{1, \ldots, n\}$.

Finally, we revisit our statement of sufficient conditions for equation (10), and provide coordinate formulae to test the non-degeneracy of the endpoint map ϕ_t that was defined in Theorem 2. These formulae can be evaluated by solving a system of linear, time-varying matrix differential equations, something that is easy to do using modern numerical methods. We require two lemmas before our main result in Theorem 4:

Lemma 1. *Let $q\colon U \to G$ be a smooth map, where $U \subset \mathbb{R}^2$ is simply connected. Denote its partial derivatives $\zeta\colon U \to \mathfrak{g}$ and $\eta\colon U \to \mathfrak{g}$ by*

$$\begin{aligned} \zeta(t,\epsilon) &= T_{q(t,\epsilon)} L_{q(t,\epsilon)^{-1}} \left(\frac{\partial q(t,\epsilon)}{\partial t} \right) \\ \eta(t,\epsilon) &= T_{q(t,\epsilon)} L_{q(t,\epsilon)^{-1}} \left(\frac{\partial q(t,\epsilon)}{\partial \epsilon} \right). \end{aligned} \tag{15}$$

Then,

$$\frac{\partial \zeta}{\partial \epsilon} - \frac{\partial \eta}{\partial t} = [\zeta, \eta]. \tag{16}$$

Conversely, if there exists smooth maps ζ and η satisfying equation (16)*, then there exists a smooth map q satisfying equation* (15)*.*

Proof. See Proposition 5.1 of Bloch et al. (1996). □

Lemma 2. *Let $\alpha, \beta, \gamma \in \mathfrak{g}$ and suppose $\gamma = [\alpha, \beta]$. Then*

$$\gamma_k = \sum_{r=1}^{n} \sum_{s=1}^{n} \alpha_r \beta_s C^k_{rs}.$$

Proof. This result is easily obtained from the definition in equation (14). □

Theorem 4 (Reduction of sufficient conditions)**.** *Suppose that $H \in C^\infty(T^*G)$ is left-invariant and that X_H is complete. Let $h = H|_{\mathfrak{g}^*}$ be the restriction of H to $\mathfrak{g}^*$ and let $\varphi\colon \mathbb{R} \times T^*G \to T^*G$ be the flow of X_H. Given $q_0 \in G$, define the endpoint map $\phi_t\colon T^*_{q_0}G \to G$ by $\phi_t(p) = \pi \circ \varphi(t, p, q_0)$. Given $p_0 \in T^*_{q_0}G$, let $a \in \mathbb{R}^n$ be the coordinate representation of $T^*_e L_{q_0}(p_0)$, i.e.*

$$T^*_e L_{q_0}(p_0) = \sum_{i=1}^{n} a_i P_i. \tag{17}$$

Solve the ordinary differential equations

$$\dot{\mu}_i = -\sum_{j=1}^{n} \sum_{k=1}^{n} C^k_{ij} \frac{\delta h}{\delta \mu_j} \mu_k \qquad i \in \{1, \ldots, n\} \tag{18}$$

with the initial conditions $\mu_i(0) = a_i$ for $i \in \{1, \ldots, n\}$. Define matrices $\mathbf{F}, \mathbf{G}, \mathbf{H} \in \mathbb{R}^{n \times n}$ as follows:

$$\begin{aligned} [\mathbf{F}]_{ij} &= -\frac{\partial}{\partial \mu_j} \sum_{r=1}^{n} \sum_{s=1}^{n} C^s_{ir} \frac{\delta h}{\delta \mu_r} \mu_s \\ [\mathbf{G}]_{ij} &= \frac{\partial}{\partial \mu_j} \frac{\delta h}{\delta \mu_i} \\ [\mathbf{H}]_{ij} &= -\sum_{r=1}^{n} \frac{\delta h}{\delta \mu_r} C^i_{rj}. \end{aligned}$$

Solve the (linear, time-varying) matrix differential equations

$$\dot{\mathbf{M}} = \mathbf{F}\mathbf{M} \tag{19}$$

$$\dot{\mathbf{J}} = \mathbf{G}\mathbf{M} + \mathbf{H}\mathbf{J} \tag{20}$$

with initial conditions $\mathbf{M}(0) = I$ and $\mathbf{J}(0) = 0$. The endpoint map ϕ_t is degenerate at p_0 if and only if $\det(\mathbf{J}(t)) = 0$.

Proof. Define the smooth map $\rho\colon \mathbb{R}^n \to T^*_{q_0}G$ by

$$\rho(a) = T^*_{q_0} L^{-1}_{q_0} \left(\sum_{i=1}^{n} a_i P_i \right).$$

This same expression defines $\rho\colon \mathbb{R}^n \to T_{p_0}(T^*_{q_0}G)$ if we identify $T^*_{q_0}G$ with $T_{p_0}(T^*_{q_0}G)$ in the usual way. Given $p_0 = \rho(a)$ for some $a \in \mathbb{R}^n$, there exists non-zero $\lambda \in T_{p_0}(T^*_{q_0}G)$ satisfying $T_{p_0}\phi_t(\lambda) = 0$ if and only if there exists non-zero $s \in \mathbb{R}^n$ satisfying $T_{\rho(a)}\phi_t(\rho(s)) = 0$. Define the smooth map $q\colon [0,1]\times\mathbb{R}^n \to G$ by $q(t,a) = \phi_t \circ \rho(a)$. Noting that

$$\frac{\partial q(t,a)}{\partial a_j} = T_{\rho(a)}\phi_t\left(T^*_{q_0}L_{q_0^{-1}}(P_j)\right)$$

for $j \in \{1,\ldots,n\}$, we have

$$T_{\rho(a)}\phi_t(\rho(s)) = \sum_{j=1}^{n} s_j \frac{\partial q(t,a)}{\partial a_j}.$$

By left translation, $T_{\rho(a)}\phi_t(\rho(s)) = 0$ if and only if

$$0 = \sum_{j=1}^{n} s_j T_{q(t,a)}L_{q(t,a)^{-1}}\left(\frac{\partial q(t,a)}{\partial a_j}\right). \tag{21}$$

For each $j \in \{1,\ldots,n\}$, let

$$\eta^j(t,a) = T_{q(t,a)}L_{q(t,a)^{-1}}\left(\frac{\partial q(t,a)}{\partial a_j}\right).$$

Define $\mathbf{J}\colon [0,1] \to \mathbb{R}^{n\times n}$ so that $\mathbf{J}(t)$ has entries

$$[\mathbf{J}]_{ij} = \eta^j_i(t,a),$$

i.e. the jth column of $\mathbf{J}(t)$ is the coordinate representation of $\eta^j(t,a)$ with respect to $\{X_1,\ldots,X_n\}$. Then, equation (21) holds for some $s \neq 0$ if and only if $\det(\mathbf{J}(t)) = 0$. We conclude that ϕ_t is degenerate at p_0 if and only if $\det(\mathbf{J}(t)) = 0$.

It remains to show that $\mathbf{J}(t)$ can be computed as described in the theorem. Taking $\mu_1(t),\ldots,\mu_n(t)$ as coordinates of $\mu(t)$, it is easy to verify that equations (13) and (18) are equivalent (see Marsden and Ratiu (1999)). We extend each coordinate function in the obvious way to $\mu_i\colon [0,1]\times\mathbb{R}^n \to \mathbb{R}$, so $\mu_i(t,a)$ solves equation (18) with initial condition $\mu_i(0,a) = a_i$. Define $\mathbf{M}\colon [0,1] \to \mathbb{R}^{n\times n}$ by

$$[\mathbf{M}(t)]_{ij} = \partial\mu_i/\partial a_j.$$

Differentiating equation (18), we compute

$$\begin{aligned}[\dot{\mathbf{M}}]_{ij} &= \frac{\partial}{\partial t}\frac{\partial \mu_i}{\partial a_j} = \frac{\partial}{\partial a_j}\frac{\partial \mu_i}{\partial t} = \frac{\partial}{\partial a_j}\left(-\sum_{r=1}^{n}\sum_{s=1}^{n} C^s_{ir}\frac{\delta h}{\delta \mu_r}\mu_s\right)\\ &= \sum_{k=1}^{n} -\frac{\partial}{\partial \mu_k}\left(\sum_{r=1}^{n}\sum_{s=1}^{n} C^s_{ir}\frac{\delta h}{\delta \mu_r}\mu_s\right)\frac{\partial \mu_k}{\partial a_j}\\ &= \sum_{k=1}^{n}[\mathbf{F}]_{ik}[\mathbf{M}]_{kj}.\end{aligned}$$

It is clear that $[\mathbf{M}(0)]_{ij} = \delta_{ij}$, so we have verified equation (19). Next, define

$$\zeta(t,a) = T_{q(t,a)}L_{q(t,a)^{-1}}\left(\frac{\partial q(t,a)}{\partial t}\right).$$

We have

$$\dot{\eta}^j = \frac{\partial \zeta}{\partial a_j} - \left[\zeta, \eta^j\right] = \frac{\partial}{\partial a_j}\frac{\delta h}{\delta \mu} - \left[\frac{\delta h}{\delta \mu}, \eta^j\right]$$

from Lemma 1 and Theorem 3. We write this equation in coordinates by application of Lemma 2:

$$\begin{aligned}[\dot{\mathbf{J}}]_{ij} = \dot{\eta}^j_i &= \sum_{k=1}^{n}\left(\frac{\partial}{\partial \mu_k}\frac{\delta h}{\delta \mu_i}\right)\frac{\partial \mu_k}{\partial a_j} + \sum_{k=1}^{n}\left(-\sum_{r=1}^{n}\frac{\delta h}{\delta \mu_r}C^i_{rk}\right)\eta^j_k\\ &= \sum_{k=1}^{n}[\mathbf{G}]_{ik}[\mathbf{M}]_{kj} + \sum_{k=1}^{n}[\mathbf{H}]_{ik}[\mathbf{J}]_{kj}.\end{aligned}$$

It is clear that $[\mathbf{J}(0)]_{ij} = 0$, so we have verified equation (20). □

5. Mechanics of an elastic rod

The previous section derived coordinate formulae to compute necessary and sufficient conditions for a particular class of optimal control problems on manifolds. Here, we apply these formulae to a Kirchhoff elastic rod.

We begin with three results that suffice to describe all possible configurations of the rod that can be achieved by quasi-static manipulation. Section 5.1 recalls that any framed curve traced by the rod in static equilibrium can be described as a local solution to a geometric optimal control problem (Walsh et al., 1994; Biggs et al., 2007). Section 5.2 proves that the set of all trajectories that are normal with respect to this problem is a smooth manifold of finite dimension that can be parameterized by a single chart (Theorem 6). Section 5.3 proves that the set of all normal trajectories that are also local optima is an open subset of this smooth manifold, and provides a computational test for membership in this subset (Theorem 7).

We conclude with two additional results that, as we will see in Section 6, are useful in the context of a sampling-based planning algorithm for manipulation planning. Section 5.4 provides a physical interpretation of the coordinate chart we derive as a space of moments and forces. Section 5.5 defines a "straight-line path" in both this chart and in the space of boundary conditions.

5.1. Model

We refer to the object in Figure 1 as a *rod*. Assuming that it is thin, inextensible, and of unit length, we describe the shape of this rod by a continuous map $q\colon [0,1] \to G$, where $G = SE(3)$. Abbreviating $T_eL_q(\zeta) = q\zeta$ as usual for matrix Lie groups, we require this map to satisfy

$$\dot{q} = q(u_1X_1 + u_2X_2 + u_3X_3 + X_4) \tag{22}$$

for some $u\colon [0,1] \to U$, where $U = \mathbb{R}^3$ and

$$X_1 = \begin{bmatrix} 0&0&0&0 \\ 0&0&-1&0 \\ 0&1&0&0 \\ 0&0&0&0 \end{bmatrix} X_2 = \begin{bmatrix} 0&0&1&0 \\ 0&0&0&0 \\ -1&0&0&0 \\ 0&0&0&0 \end{bmatrix} X_3 = \begin{bmatrix} 0&-1&0&0 \\ 1&0&0&0 \\ 0&0&0&0 \\ 0&0&0&0 \end{bmatrix}$$

$$X_4 = \begin{bmatrix} 0&0&0&1 \\ 0&0&0&0 \\ 0&0&0&0 \\ 0&0&0&0 \end{bmatrix} X_5 = \begin{bmatrix} 0&0&0&0 \\ 0&0&0&1 \\ 0&0&0&0 \\ 0&0&0&0 \end{bmatrix} X_6 = \begin{bmatrix} 0&0&0&0 \\ 0&0&0&0 \\ 0&0&0&1 \\ 0&0&0&0 \end{bmatrix}$$

is a basis for $\mathfrak{g}$. Denote the dual basis for $\mathfrak{g}^*$ by $\{P_1, \ldots, P_6\}$. We refer to q and u together as $(q,u) : [0,1] \to G \times U$ or simply as (q,u). Each end of the rod is held by a robotic gripper. We ignore the structure of these grippers, and simply assume that they fix arbitrary $q(0)$ and $q(1)$. We further assume, without loss of generality, that $q(0) = e$. We denote the space of all possible $q(1)$ by $\mathcal{B} = G$. Finally, we assume that the rod is elastic in the sense of Kirchhoff (Biggs et al., 2007), so has total elastic energy

$$\frac{1}{2}\int_0^1 \left(c_1 u_1^2 + c_2 u_2^2 + c_3 u_3^2\right) \mathrm{d}t$$

for given constants $c_1, c_2, c_3 > 0$. For fixed endpoints, the rod will be motionless only if its shape locally minimizes the total elastic energy. In particular, we say that (q,u) is in static equilibrium if it is a local optimum of

$$\begin{aligned} \underset{q,u}{\text{minimize}} \quad & \frac{1}{2}\int_0^1 \left(c_1 u_1^2 + c_2 u_2^2 + c_3 u_3^2\right) \mathrm{d}t \\ \text{subject to} \quad & \dot{q} = q(u_1 X_1 + u_2 X_2 + u_3 X_3 + X_4) \\ & q(0) = e, \qquad q(1) = b \end{aligned} \tag{23}$$

for some $b \in \mathcal{B}$.

5.2. Necessary conditions for static equilibrium

We have seen that if a Kirchhoff elastic rod is in static equilibrium, then its configuration (q,u) must be a local solution to the geometric optimal control problem in equation (23). In this section, we apply the necessary conditions for optimality to show that the set of all normal (q,u) is a smooth 6-manifold that can be parameterized by a single chart. Coordinates for this chart are given by the open subset $\mathcal{A} \subset \mathbb{R}^6$ that is defined by equation (27) in the following theorem. Our main result is then Theorem 6.

Theorem 5. *A trajectory (q,u) is normal with respect to equation (23) if and only if there exists $\mu\colon [0,1] \to \mathfrak{g}^*$ that satisfies*

$$\begin{aligned} \dot{\mu}_1 &= u_3\mu_2 - u_2\mu_3 & \dot{\mu}_4 &= u_3\mu_5 - u_2\mu_6 \\ \dot{\mu}_2 &= \mu_6 + u_1\mu_3 - u_3\mu_1 & \dot{\mu}_5 &= u_1\mu_6 - u_3\mu_4 \\ \dot{\mu}_3 &= -\mu_5 + u_2\mu_1 - u_1\mu_2 & \dot{\mu}_6 &= u_2\mu_4 - u_1\mu_5, \end{aligned} \tag{24}$$

$$\dot{q} = q(u_1 X_1 + u_2 X_2 + u_3 X_3 + X_4), \tag{25}$$

$$u_i = c_i^{-1}\mu_i \quad \textit{for all } i \in \{1,2,3\}, \tag{26}$$

with initial conditions $q(0) = e$ and $\mu(0) = \sum_{i=1}^6 a_i P_i$ for some $a \in \mathcal{A}$, where

$$\mathcal{A} = \left\{ a \in \mathbb{R}^6 \colon (a_2, a_3, a_5, a_6) \neq (0,0,0,0) \right\}. \tag{27}$$

Proof. We begin by showing that (q,u) is abnormal if and only if $u_2 = u_3 = 0$. Theorem 1 tells us that (q,u) is abnormal if and only if it is the projection of an integral curve (p,q) of X_H that satisfies equation (11), where

$$H(p,q,t) = \widehat{H}(p,q,0,u(t))$$

and

$$\widehat{H}(p,q,0,u) = \langle p, q(u_1 X_1 + u_2 X_2 + u_3 X_3 + X_4) \rangle .$$

For any $g, r \in G$ satisfying $q = gr$, we compute

$$\begin{aligned} & H(T_r^* L_g(p), r, t) \\ &= \left\langle T_r^* L_g(p), g^{-1} q(u_1 X_1 + u_2 X_2 + u_3 X_3 + X_4) \right\rangle \\ &= \left\langle p, g\left(g^{-1} q(u_1 X_1 + u_2 X_2 + u_3 X_3 + X_4)\right) \right\rangle \\ &= \langle p, q(u_1 X_1 + u_2 X_2 + u_3 X_3 + X_4) \rangle \\ &= H(p,q,t), \end{aligned} \tag{28}$$

so H is left-invariant. As a consequence, the existence of (p,q) satisfying the conditions of Theorem 1 is equivalent to the existence of μ satisfying the conditions of Theorem 3:

$$\dot{\mu} = \mathrm{ad}^*_{\delta h/\delta \mu}(\mu) \qquad \text{and} \qquad \dot{q} = q(\delta h/\delta \mu),$$

where $h = H|_{\mathfrak{g}^*}$. Application of equation (18) produces the formulae in equations (24)–(25), where we require $\mu_1 = \mu_2 = \mu_3 = 0$ to satisfy equation (11). We therefore have $\dot{\mu}_2 = \mu_6$ and $\dot{\mu}_3 = -\mu_5$, hence $\mu_5 = \mu_6 = 0$. Applying this result again to equation (24), we find $\dot{\mu}_5 = -u_3\mu_4 = 0$ and $\dot{\mu}_6 = u_2\mu_4 = 0$. Since μ cannot vanish when $k = 0$, we must have $\mu_4 \neq 0$, hence $u_2 = u_3 = 0$, with u_1 an arbitrary integrable function. Our result follows.

Now, we return to the normal case. As before, Theorem 1 tells us that (q,u) is normal if and only if it is not abnormal and it is the projection of an integral curve (p,q) of X_H that satisfies equation (11), where

$$H(p,q,t) = \widehat{H}(p,q,1,u(t))$$

and

$$\begin{aligned} \widehat{H}(p,q,1,u) = {} & \langle p, q(u_1 X_1 + u_2 X_2 + u_3 X_3 + X_4) \rangle \\ & - \left(c_1 u_1^2 + c_2 u_2^2 + c_3 u_3^2\right)/2. \end{aligned}$$

By a computation identical to equation (28), H is left-invariant. Application of equation (18) to the conditions of Theorem 3 produces the same formulae in equations (24)–(25), where equation (26) follows from equation (11) because $\widehat{H}$ is quadratic in u. It remains to show that trajectories produced by equations (24)–(26) are not abnormal if and only if $a \in \mathcal{A}$. We prove the converse. First, assume $a \in \mathbb{R}^6 \backslash \mathcal{A}$, so $(a_2, a_3, a_5, a_6) = (0,0,0,0)$. From equations

(24) and (26), we see that $u_2 = u_3 = 0$, hence (q, u) is abnormal. Now, assume (q, u) is abnormal, so $u_2 = u_3 = 0$. From equation (26), we therefore have $\mu_2 = \mu_3 = 0$, and in particular $a_2 = a_3 = 0$. Plugging this result into equation (24), we see that $\dot{\mu}_2 = \mu_6$ and $\dot{\mu}_3 = -\mu_5$, hence also that $\mu_5 = \mu_6 = 0$, i.e. that $a_5 = a_6 = 0$. So, $a \in \mathbb{R}^6 \backslash \mathcal{A}$. Our result follows. □

Theorem 5 provides a set of candidates for local optima of equation (23), which we now characterize. Denote the set of all smooth maps $(q, u) : [0, 1] \to G \times U$ under the smooth topology[2] by $C^\infty([0, 1], G \times U)$. Let

$$\mathcal{C} \subset C^\infty([0, 1], G \times U)$$

be the subset of all (q, u) that satisfy Theorem 5. Any such $(q, u) \in \mathcal{C}$ is completely defined by the choice of $a \in \mathcal{A}$, as is the corresponding μ. Denote the resulting maps by

$$\Psi(a) = (q, u) \qquad \Gamma(a) = \mu.$$

We require three lemmas before our main result in Theorem 6.

Lemma 3. *If $\Psi(a) = \Psi(a')$ for some $a, a' \in \mathcal{A}$, then $a = a'$.*

Proof. Suppose $(q, u) = \Psi(a)$ and $\mu = \Gamma(a)$ for some $a \in \mathcal{A}$. It suffices to show that a is uniquely defined by u (and its derivatives, since u is clearly smooth). From equation (26), we have

$$\begin{aligned} a_1 &= c_1 u_1(0) \\ a_2 &= c_2 u_2(0) \\ a_3 &= c_3 u_3(0). \end{aligned} \tag{29}$$

From equation (24), we have

$$\begin{aligned} a_5 &= -c_3 \dot{u}_3(0) + a_1 a_2 (c_2^{-1} - c_1^{-1}) \\ a_6 &= c_2 \dot{u}_2(0) - a_1 a_3 (c_1^{-1} - c_3^{-1}). \end{aligned} \tag{30}$$

It is now possible to compute $\dot{\mu}_i(0)$ and $\ddot{\mu}_i(0)$ for $i \in \{4, 5, 6\}$ by differentiation of

$$\begin{aligned} \dot{\mu}_4 &= u_3 \mu_5 - u_2 \mu_6 \\ \mu_5 &= -\dot{\mu}_3 + u_2 \mu_1 - u_1 \mu_2 \\ \mu_6 &= \dot{\mu}_2 - u_1 \mu_3 - u_3 \mu_1, \end{aligned} \tag{31}$$

where we use equation (26) to find derivatives of $\mu_i(0)$ for $i \in \{1, 2, 3\}$. Based on these results, we differentiate equation (24) again to produce

$$\begin{aligned} &(c_3^{-1} a_3)\, a_4 = c_1^{-1} a_1 a_6 - \dot{\mu}_5(0) \\ &(c_2^{-1} a_2)\, a_4 = c_1^{-1} a_1 a_5 + \dot{\mu}_6(0) \\ &(-a_5 + a_1 a_2 (c_2^{-1} - c_1^{-1}))\, a_4 = c_3 (c_1^{-1} (\dot{\mu}_1(0)\, a_6 \\ &\quad + a_1 \dot{\mu}_6(0)) - \ddot{\mu}_5(0)) - a_3 \dot{\mu}_4(0) \\ &(a_6 + a_1 a_3 (c_1^{-1} - c_3^{-1})\, a_4 = c_2 (c_1^{-1} (\dot{\mu}_1(0)\, a_5 \\ &\quad + a_1 \dot{\mu}_5(0)) + \ddot{\mu}_6(0)) - a_2 \dot{\mu}_4(0). \end{aligned} \tag{32}$$

At least one of these four equations allows us to compute a_4 unless

$$(a_2, a_3, a_5, a_6) = (0, 0, 0, 0),$$

which would violate our assumption that $a \in \mathcal{A}$. Our result follows. □

Lemma 4. *The map $\Psi : \mathcal{A} \to \mathcal{C}$ is a homeomorphism.*

Proof. The map Ψ is clearly a bijection—it is well-defined and onto by construction, and is one-to-one by Lemma 3. Continuity of Ψ also follows immediately from Theorem 5.

It remains only to show that $\Psi^{-1} : \mathcal{C} \to \mathcal{A}$ is continuous. This result is a corollary to the proof of Lemma 3. From equation (29), we see that a_1, a_2, a_3 depend continuously on $u(0)$. From equation (30), we see that a_5, a_6 depend continuously on $a_1, a_2, a_3, \dot{u}(0)$, hence on $u(0), \dot{u}(0)$. From equation (31), we see in the same way that $\dot{\mu}_4(0), \dot{\mu}_5(0), \dot{\mu}_6(0), \ddot{\mu}_5(0), \ddot{\mu}_6(0)$ depend continuously on $u(0), \dot{u}(0), \ddot{u}(0)$. Hence, all of the quantities in equation (32) depend continuously on $u(0), \dot{u}(0), \ddot{u}(0)$, so a_4 does as well. Our result follows. □

Lemma 5. *If the topological n-manifold M has an atlas consisting of the single chart (M, α), then $N = \alpha(M)$ is a topological n-manifold with an atlas consisting of the single chart (N, id_N), where id_N is the identity map. Furthermore, both M and N are smooth n-manifolds and $\alpha : M \to N$ is a diffeomorphism.*

Proof. Since (M, α) is a chart, then N is an open subset of $\mathbb{R}^n$ and α is a bijection. Hence, our first result is immediate and our second result requires only that both α and α^{-1} are smooth maps. For every $p \in M$, the charts (M, α) and (N, id_N) satisfy $\alpha(p) \in N$, $\alpha(M) = N$, and $\mathrm{id}_N \circ \alpha \circ \alpha^{-1} = \mathrm{id}_N$, so α is a smooth map. For every $q \in N$, the charts (N, id_N) and (M, α) again satisfy $\alpha^{-1}(q) \in M$, $\alpha^{-1}(N) = M$, and $\alpha \circ \alpha^{-1} \circ \mathrm{id}_N = \mathrm{id}_N$, so α^{-1} is also a smooth map. Our result follows. □

Theorem 6. *$\mathcal{C}$ is a smooth 6-manifold with smooth structure determined by an atlas with the single chart $(\mathcal{C}, \Psi^{-1})$.*

Proof. Since $\Psi : \mathcal{A} \to \mathcal{C}$ is a homeomorphism by Lemma 4 and $\mathcal{A} \subset \mathbb{R}^6$ is open, then $(\mathcal{C}, \Psi^{-1})$ is a chart whose domain is $\mathcal{C}$. Our result follows from Lemma 5. □

5.3. Sufficient conditions for static equilibrium

As we have seen, any trajectory (q, u) that is normal with respect to the optimal control problem equation (23) can be represented in coordinates by a point $a \in \mathcal{A}$. In this section, we show that any such point a produces a local optimum $\Psi(a)$ of equation (23) if and only if it is an element of a particular open subset $\mathcal{A}_{\text{stable}} \subset \mathcal{A}$. In particular, the following theorem provides a computational test for membership in this subset:

Theorem 7. *Let $(q, u) = \Psi(a)$ and $\mu = \Gamma(a)$ for some $a \in \mathcal{A}$. Define*

$$\mathbf{F} = \begin{bmatrix} 0 & \mu_3(c_3^{-1} - c_2^{-1}) & \mu_2(c_3^{-1} - c_2^{-1}) & 0 & 0 & 0 \\ \mu_3(c_1^{-1} - c_3^{-1}) & 0 & \mu_1(c_1^{-1} - c_3^{-1}) & 0 & 0 & 1 \\ \mu_2(c_2^{-1} - c_1^{-1}) & \mu_1(c_2^{-1} - c_1^{-1}) & 0 & 0 & -1 & 0 \\ 0 & -\mu_6/c_2 & \mu_5/c_3 & 0 & \mu_3/c_3 & -\mu_2/c_2 \\ \mu_6/c_1 & 0 & -\mu_4/c_3 & -\mu_3/c_3 & 0 & \mu_1/c_1 \\ -\mu_5/c_1 & \mu_4/c_2 & 0 & \mu_2/c_2 & -\mu_1/c_1 & 0 \end{bmatrix}$$

$$\mathbf{G} = \operatorname{diag}\left(c_1^{-1}, c_2^{-1}, c_3^{-1}, 0, 0, 0\right)$$

$$\mathbf{H} = \begin{bmatrix} 0 & \mu_3/c_3 & -\mu_2/c_2 & 0 & 0 & 0 \\ -\mu_3/c_3 & 0 & \mu_1/c_1 & 0 & 0 & 0 \\ \mu_2/c_2 & -\mu_1/c_1 & 0 & 0 & 0 & 0 \\ 0 & 0 & 0 & 0 & \mu_3/c_3 & -\mu_2/c_2 \\ 0 & 0 & 1 & -\mu_3/c_3 & 0 & \mu_1/c_1 \\ 0 & -1 & 0 & \mu_2/c_2 & -\mu_1/c_1 & 0 \end{bmatrix}.$$

Solve the (linear, time-varying) matrix differential equations

$$\begin{aligned} \dot{\mathbf{M}} &= \mathbf{F}\mathbf{M} \\ \dot{\mathbf{J}} &= \mathbf{G}\mathbf{M} + \mathbf{H}\mathbf{J} \end{aligned} \tag{33}$$

with initial conditions $\mathbf{M}(0) = I$ *and* $\mathbf{J}(0) = 0$. *Then,* (q, u) *is a local optimum of equation* (23) *for* $b = q(1)$ *if and only if* $\det(\mathbf{J}(t)) \neq 0$ *for all* $t \in (0, 1]$.

Proof. As we have already seen, normal extremals of equation (23) are derived from the parameterized Hamiltonian function

$$\begin{aligned} \widehat{H}(p, q, 1, u) = \langle p, q(u_1 X_1 + u_2 X_2 + u_3 X_3 + X_4) \rangle \\ -\frac{1}{2}\left(c_1 u_1^2 + c_2 u_2^2 + c_3 u_3^2\right). \end{aligned}$$

This function satisfies

$$\frac{\partial^2 \widehat{H}}{\partial u^2} = -\operatorname{diag}(c_1, c_2, c_3) < 0$$

and admits a unique maximum at

$$u_i = c_i^{-1} \langle p, q X_i \rangle$$

for $i \in \{1, 2, 3\}$. The maximized Hamiltonian function is

$$H(p, q) = \frac{1}{2} \sum_{i=1}^{3} c_i^{-1} \langle p, q X_i \rangle^2 + \langle p, q X_4 \rangle.$$

It is clear that X_H is complete. By Lemma 3, the mapping from (q, u) to a and hence to $\mu = \Gamma(a)$ is unique. By Theorem 3, it is equivalent that the mapping from (q, u) to (p, q) is unique. As a consequence, we may apply Theorem 2 to establish sufficient conditions for optimality. Since a computation identical to equation (28) shows that H is left-invariant, we may apply the equivalent conditions of Theorem 4. Noting that the restriction $h = H|_{\mathfrak{g}^*} \in C^\infty(\mathfrak{g}^*)$ is given by

$$h(\mu) = \frac{1}{2}\left(\frac{\mu_1^2}{c_1} + \frac{\mu_2^2}{c_2} + \frac{\mu_3^2}{c_3}\right) + \mu_4,$$

it is easy to verify that $\mathbf{F}$, $\mathbf{G}$ and $\mathbf{H}$ take the form given above. Our result follows. □

As we have said, Theorem 7 provides a computational test of which points $a \in \mathcal{A}$ actually produce local optima $\Psi(a) \in \mathcal{C}$ of equation (23). Let

$$\mathcal{A}_{\text{stable}} \subset \mathcal{A}$$

be the subset of all a for which the conditions of Theorem 7 are satisfied and let

$$\mathcal{C}_{\text{stable}} = \Psi(\mathcal{A}_{\text{stable}}) \subset \mathcal{C}.$$

An important consequence of membership in $\mathcal{A}_{\text{stable}}$ is smooth local dependence of solutions to equation (23) on variation in b. Define

$$\begin{aligned} \mathcal{B}_{\text{stable}} = \{ b \in \mathcal{B} : \text{there exists } (q, u) \in \mathcal{C}_{\text{stable}} \\ \text{for which } q(1) = b \}. \end{aligned}$$

Let $\Phi : \mathcal{C} \to \mathcal{B}$ be the map taking (q, u) to $q(1)$. Clearly $\mathcal{A}_{\text{stable}}$ is open, so

$$\Psi|_{\mathcal{A}_{\text{stable}}} : \mathcal{A}_{\text{stable}} \to \mathcal{C}_{\text{stable}}$$

is a diffeomorphism. We arrive at the following result:

Theorem 8. *The map*

$$\Phi \circ \Psi|_{\mathcal{A}_{\text{stable}}} : \mathcal{A}_{\text{stable}} \to \mathcal{B}_{\text{stable}}$$

is a local diffeomorphism.

Proof. The map $\Phi \circ \Psi|_{\mathcal{A}_{\text{stable}}}$ is smooth and by Theorem 7 has non-singular Jacobian matrix $\mathbf{J}(1)$. Our result follows from the Implicit Function Theorem (Lee, 2003, Theorem 7.9). □

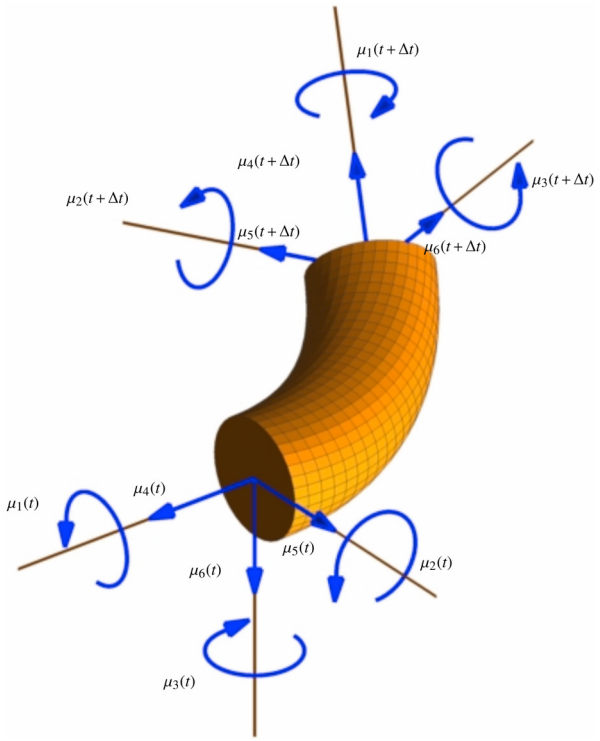

Fig. 5. Forces (μ_4, μ_5, μ_6) and torques (μ_1, μ_2, μ_3) applied to a piece of the elastic rod, providing a physical interpretation of the co-state trajectory.

5.4. Physical interpretation of $\mathcal{A}$

In this section, we derive equations (24) and (26) in another way that gives a physical interpretation of the coordinate chart

$$\mathcal{A} = \left\{ a \in \mathbb{R}^6 \colon (a_2, a_3, a_5, a_6) \neq (0,0,0,0) \right\}.$$

Given the integral curve $\mu \colon [0,1] \to \mathfrak{g}^*$, define

$$\mathbf{m}(t) = \begin{bmatrix} \mu_1(t) \\ \mu_2(t) \\ \mu_3(t) \end{bmatrix} \quad \text{and} \quad \mathbf{f}(t) = \begin{bmatrix} \mu_4(t) \\ \mu_5(t) \\ \mu_6(t) \end{bmatrix}$$

for $t \in [0,1]$. We will show that $\mathbf{m}(t)$ and $\mathbf{f}(t)$ describe moment and force, respectively, acting on the rod at any cut $t \in [0,1]$, both expressed in the local coordinates defined by $q(t)$. Consider a piece of the rod corresponding to the interval $[t, t+\Delta t] \subset [0,1]$, as shown in Figure 5. Define $R \in SO(3)$ and $v \in \mathbb{R}^3$ so that

$$\begin{bmatrix} R & v \\ 0 & 1 \end{bmatrix} = q(t)^{-1} q(t+\Delta t).$$

If our interpretation of $\mathbf{m}$ and $\mathbf{f}$ is correct, then—in static equilibrium—a force and moment balance requires

$$\begin{aligned} -\mathbf{f}(t) + R\,\mathbf{f}(t+\Delta t) &= 0 \\ -\mathbf{m}(t) + R\,(\mathbf{m}(t+\Delta t) + \widehat{v}\,\mathbf{f}(t+\Delta t)) &= 0, \end{aligned} \tag{34}$$

where "$\widehat{\cdot}$" is the mapping

$$\widehat{v} = \begin{bmatrix} 0 & -v_3 & v_2 \\ v_3 & 0 & -v_1 \\ -v_2 & v_1 & 0 \end{bmatrix}$$

that implements a cross product (see Murray et al. (1994)). For small Δt, we approximate equation (34) to first order as

$$\begin{aligned} &-\mathbf{f}(t) + \mathbf{f}(t+\Delta t) + \Delta t \left(\widehat{u(t)}\,\mathbf{f}(t+\Delta t) \right) \approx 0 \\ &-\mathbf{m}(t) + \mathbf{m}(t+\Delta t) + \Delta t (\widehat{u(t)}\,\mathbf{m}(t+\Delta t) \\ &\quad + \widehat{\mathbf{e}_1}\,\mathbf{f}(t+\Delta t)) \approx 0, \end{aligned} \tag{35}$$

where

$$\mathbf{e}_1 = \begin{bmatrix} 1 \\ 0 \\ 0 \end{bmatrix}.$$

This result may be obtained, for example, by taking a series expansion of equation (34) about $\Delta t \approx 0$. As a consequence, we have

$$\begin{aligned} \dot{\mathbf{f}}(t) &= \lim_{\Delta t \to 0} \frac{\mathbf{f}(t+\Delta t) - \mathbf{f}(t)}{\Delta t} \\ &= \lim_{\Delta t \to 0} \left(-\widehat{u(t)}\,\mathbf{f}(t+\Delta t) \right) \\ &= -\widehat{u(t)}\,\mathbf{f}(t) \end{aligned}$$

and

$$\begin{aligned} \dot{\mathbf{m}}(t) &= \lim_{\Delta t \to 0} \frac{\mathbf{m}(t+\Delta t) - \mathbf{m}(t)}{\Delta t} \\ &= \lim_{\Delta t \to 0} \left(-\widehat{u(t)}\,\mathbf{m}(t+\Delta t) - \widehat{\mathbf{e}_1}\,\mathbf{f}(t+\Delta t) \right) \\ &= -\widehat{u(t)}\,\mathbf{m}(t) - \widehat{\mathbf{e}_1}\,\mathbf{f}(t). \end{aligned}$$

The reader may verify that these results are exactly the same as equation (24). Equation (26) then follows from the linear relationship between stress and strain, which—for a Kirchhoff elastic rod—requires that

$$\mathbf{m}(t) = \operatorname{diag}(c_1, c_2, c_3)\, u(t)$$

for some $c_1, c_2, c_3 > 0$.

It is now clear that $\mathcal{A}$ is a space of moments and forces, and in particular that $\mu(0) = a \in \mathcal{A}$ represents the moment $\mathbf{m}(0)$ and force $\mathbf{f}(0)$ at the base of a Kirchhoff elastic rod. We note that abnormal (q,u), generated by $a \in \mathbb{R}^6 \backslash \mathcal{A}$, are exactly those configurations of the rod at which $\mathbf{m}(0)$ and $\mathbf{f}(0)$ are indeterminate. This interpretation is entirely classical (Antman, 2005)—the reader may compare it to the usual relationship between generalized forces and Lagrange multipliers. We will use this interpretation in Section 6 to justify our choice of sampling strategy for manipulation planning.

Before proceeding, we also note that the curvature κ and torsion τ of the curve that is traced by the elastic rod are given by

$$\begin{aligned} \kappa^2 &= \mu_2^2 + \mu_3^2 \\ \tau &= \mu_1 - \left(\frac{\mu_2 \mu_5 + \mu_3 \mu_6}{\mu_2^2 + \mu_3^2} \right), \end{aligned}$$

in the special case $c_1 = c_2 = c_3 = 1$ (see Biggs et al. (2007)). It is easy to verify that

$$\begin{aligned} 2\ddot{\kappa} + \kappa^3 - 2\kappa(\tau - \lambda_1)^2 &= \lambda_2\kappa \\ \kappa^2(\tau - \lambda_1) &= \lambda_3 \end{aligned} \tag{36}$$

and equations (24)–(26) are equivalent, where

$$\begin{aligned} \lambda_1 &= \frac{\mu_1(0)}{2} \\ \lambda_2 &= \kappa(0)^2 + 2\mu_4(0) - \frac{\mu_1(0)^2}{2} \\ \lambda_3 &= \kappa(0)^2\left(\tau(0) - \frac{\mu_1(0)}{2}\right) \end{aligned}$$

are constants of integration. In this way, we recover the variational constraints in equation (36) that would have been produced by analysis of equation (23) from a Lagrangian perspective (Shi and Hearst, 1994; Langer and Singer, 1996; Shi et al., 1998).

5.5. Straight-line paths in $\mathcal{A}$ and $\mathcal{B}$

In this section, we show how to compute "straight-line paths" in both the chart $\mathcal{A}$ that we have derived and the space $\mathcal{B}$ of boundary conditions. We will use these paths as alternative local connection strategies in the sampling-based planning algorithm of Section 6.

$\mathcal{A}$-Connected Let $a_{\text{start}}, a_{\text{goal}} \in \mathcal{A}_{\text{stable}}$. We say that a_{start} and a_{goal} are *$\mathcal{A}$-connected* if

$$a_{\text{start}} + s\left(a_{\text{goal}} - a_{\text{start}}\right) \in \mathcal{A}_{\text{stable}}$$

for $s \in [0, 1]$. It is equivalent to say that a_{start} and a_{goal} are connected by a straight-line path in $\mathcal{A}_{\text{stable}}$.

$\mathcal{B}$-Connected Let

$$\begin{aligned} b_{\text{start}} &= \Phi \circ \Psi|_{\mathcal{A}_{\text{stable}}}(a_{\text{start}}) \\ b_{\text{goal}} &= \Phi \circ \Psi|_{\mathcal{A}_{\text{stable}}}(a_{\text{goal}}) \end{aligned}$$

for some $a_{\text{start}}, a_{\text{goal}} \in \mathcal{A}_{\text{stable}}$. Define $R \in SO(3)$ and $v \in \mathbb{R}^3$ so that

$$\begin{bmatrix} R & v \\ 0 & 1 \end{bmatrix} = b_{\text{start}}^{-1} b_{\text{goal}}.$$

Define exponential coordinates $w \in \mathbb{R}^3$ and $\theta \in [0, \pi)$ for R in the usual way (Murray et al., 1994), taking $w = 0$ when $R = I$. Define $\beta : [0, 1] \to \mathcal{B}$ by

$$\beta(s) = b_{\text{start}} \begin{bmatrix} \exp(s\widehat{w}\theta) & sv \\ 0 & 1 \end{bmatrix}.$$

Assume that $\beta(s) \in \mathcal{B}_{\text{stable}}$ for all $s \in [0, 1]$. Recall from Theorem 8 that

$$\Phi \circ \Psi|_{\mathcal{A}_{\text{stable}}} : \mathcal{A}_{\text{stable}} \to \mathcal{B}_{\text{stable}}$$

is a local diffeomorphism with non-singular Jacobian matrix $\mathbf{J}(1)$. This matrix, of course, depends on the argument $a \in \mathcal{A}_{\text{stable}}$. In what follows, we make this dependence explicit by writing $\mathbf{J}_a(1)$. Let $\alpha : [0, 1] \to \mathcal{A}$ be the solution to

$$\frac{d\alpha}{ds} = (\mathbf{J}_\alpha(1))^{-1} \begin{bmatrix} w\theta \\ v \end{bmatrix} \tag{37}$$

with initial condition $\alpha(0) = a_{\text{start}}$. We know that this solution exists and is unique because, again, $\Phi \circ \Psi|_{\mathcal{A}_{\text{stable}}}$ is a local diffeomorphism. By construction, we also have

$$\beta(s) = \Phi \circ \Psi|_{\mathcal{A}_{\text{stable}}} \circ \alpha(s)$$

for $s \in [0, 1]$. Note that, because $\Phi \circ \Psi|_{\mathcal{A}_{\text{stable}}}$ is only a local diffeomorphism, this result does not necessarily imply that $\alpha(1) = a_{\text{goal}}$. We say that a_{start} and a_{goal} are *$\mathcal{B}$-connected* if indeed $\alpha(1) = a_{\text{goal}}$ and if our assumption that $\beta(s) \in \mathcal{B}_{\text{stable}}$ for $s \in [0, 1]$ was correct.

6. Manipulation of an elastic rod

It is now clear how to do quasi-static manipulation planning for a Kirchhoff elastic rod. Recall that we want to find a path of the gripper that causes the rod to move between given start and goal configurations while remaining in static equilibrium. As pointed out by Lamiraux and Kavraki (2001), it is equivalent to find a path *of the rod* through its set of equilibrium configurations. What makes this problem seem hard is the apparent lack of coordinates to describe these equilibrium configurations. Section 5 has given us the coordinates that we need.

In particular, we have seen that any equilibrium configuration can be represented by a point in $\mathcal{A}_{\text{stable}} \subset \mathcal{A} \subset \mathbb{R}^6$. It is correct to think of $\mathcal{A}$ as the "configuration space" of the rod during quasi-static manipulation and of $\mathcal{A}_{\text{stable}}$ as the "free space". Theorems 5–6 say how to map points in $\mathcal{A}$ to configurations of the rod. Theorem 7 says how to test membership in $\mathcal{A}_{\text{stable}}$, i.e. it provides a "collision checker". Theorem 8 says that paths in $\mathcal{A}_{\text{stable}}$ can be "implemented" by the gripper, by establishing a well-defined map between differential changes in the rod (represented by $\mathcal{A}_{\text{stable}}$) and in the gripper (represented by $\mathcal{B}_{\text{stable}}$).

In other words, we have expressed the quasi-static manipulation planning problem for a Kirchhoff elastic rod as a standard motion planning problem in a configuration space of dimension six, for which there are hundreds of possible solution approaches (Latombe, 1991; Choset et al., 2005; LaValle, 2006).

In Section 6.1, we describe a sampling-based planning algorithm that is easy to implement. In Section 6.2, we compare this algorithm to what was suggested by the representative work of Moll and Kavraki (2006).

6.1. Sampling-based planning algorithm

Here is one way to implement a sampling-based algorithm like the Probabilistic Roadmap Method (PRM) (Kavraki et al., 1996) for quasi-static manipulation planning:

- Sample points uniformly at random in

$$\Big\{a \in \mathcal{A}\colon\ |a_i| \le m_{\max} \text{ for } i = 1,2,3 \text{ and } |a_i| \le f_{\max} \text{ for } i = 4,5,6\Big\},$$

  where $m_{\max}$ is an upper bound on allowable moments (a_1, a_2, a_3) and $f_{\max}$ is an upper bound on allowable forces (a_4, a_5, a_6) at the base of the rod (see Section 5.4).
- Add each point a as a node to the roadmap if the function FREECONF(a) returns TRUE (see Figure 6, which summarizes the computations derived in Sections 5.1–5.3 to test that $a \in \mathcal{A}_{\text{stable}}$).
- Add an edge between each pair of nodes a and a' if they are $\mathcal{A}$-connected (see Section 5.5). This test can be approximated in the usual way by sampling points along the straight-line path from a to a' at some resolution, evaluating FREECONF at each point.
- Declare $a_{\text{start}}, a_{\text{goal}} \in \mathcal{A}_{\text{stable}}$ to be path-connected if they are connected by a sequence of nodes and edges in the roadmap. This sequence is a continuous and piecewise-smooth map

$$\alpha\colon [0,1] \to \mathcal{A}_{\text{stable}},$$

  where $\alpha(0) = a_{\text{start}}$ and $\alpha(1) = a_{\text{goal}}$.
- Move the robotic gripper along the path

$$\beta\colon [0,1] \to \mathcal{B}_{\text{stable}}$$

  defined by

$$\beta(s) = \Phi \circ \Psi|_{\mathcal{A}_{\text{stable}}} \circ \alpha(s)$$

  for $s \in [0,1]$. This path is also continuous and piecewise-smooth. It can be found by evaluating FREECONF($\alpha(s)$), which gives us $\beta(s)$ as a byproduct of checking that $\alpha(s) \in \mathcal{A}_{\text{stable}}$.

Each step is trivial with modern numerical methods. It is also easy to include other constraints within this basic framework. For example, the function FREECONF(a) in Figure 6, that we use in our own implementation, checks both that $a \in \mathcal{A}_{\text{stable}}$ and also that the configuration $(q,u) = \Psi(a)$ does not place the rod in (self-)collision. The first check is based on event location in ordinary differential equations (Shampine and Thompson, 2000) and the second check is based on bounding volume hierarchies (Gottschalk et al., 1996), modified as in Agarwal et al. (2004) for deformable linear objects.

6.2. Analysis and experimental results

The overall structure of the planning algorithm in Section 6.1 is exactly as suggested by Moll and Kavraki (2006). The key difference here is the choice of sampling and local connection strategies, and particularly the choice of *space* in which to implement these strategies. Instead of computing samples and straight-line paths in $\mathcal{B}$ (boundary conditions), we compute them in $\mathcal{A}$ (equilibrium configurations), something we can do only because of the analysis provided in Section 5.

One advantage of this choice is that points in $\mathcal{A}$ uniquely specify equilibrium configurations of the rod, which can be computed by evaluating FREECONF. Points in $\mathcal{B}$ do not uniquely specify equilibrium configurations, which in this case depend on a_{start} and on the entire path

$$\beta\colon [0,1] \to \mathcal{B}$$

taken by the gripper, and must be computed by solving a differential equation similar to equation (37). Indeed, we emphasize that "start" and "goal" for manipulation planning must be points in $\mathcal{A}_{\text{stable}}$, or equivalently points in $\mathcal{C}_{\text{stable}}$ through the diffeomorphism Ψ. It is insufficient to specify start and goal by points in $\mathcal{B}_{\text{stable}}$. We note further that planning heuristics like lazy collision-checking (Sánchez and Latombe, 2002)—which bring huge speed-ups in practice—are easy to apply when planning in $\mathcal{A}$ but hard to apply when planning in $\mathcal{B}$.

A second advantage of our choice to work in $\mathcal{A}$ is that straight-line paths in $\mathcal{A}$ are uniformly more likely to be feasible (as a function of distance) than straight-line paths in $\mathcal{B}$. Before presenting empirical results that justify this claim, we will discuss why it might be true.

Consider the example of quasi-static manipulation that is shown in Figure 1. In this case, a_{start} and a_{goal} are $\mathcal{A}$-connected, and so the algorithm in Section 6.1 produces a single straight-line path in $\mathcal{A}_{\text{stable}}$. This path is implemented by moving the gripper along the path

$$\beta\colon [0,1] \to \mathcal{B}$$

in $\mathcal{B}_{\text{stable}}$, where

$$\beta(s) = \Phi \circ \Psi|_{\mathcal{A}_{\text{stable}}} \circ \alpha(s)$$

and

$$\alpha(s) = a_{\text{start}} + s\left(a_{\text{goal}} - a_{\text{start}}\right)$$

for $s \in [0,1]$. Consider what would have happened if we had tried to plan a path from a_{start} to a_{goal} by working in the task space $\mathcal{B}$ rather than in the space $\mathcal{A}$ of equilibrium configurations. Clearly, the resulting plan cannot be represented by a single straight line in $\mathcal{B}$. We have

$$b_{\text{start}} = \Phi \circ \Psi|_{\mathcal{A}_{\text{stable}}}(a_{\text{start}}) = \Phi \circ \Psi|_{\mathcal{A}_{\text{stable}}}(a_{\text{goal}}) = b_{\text{goal}}$$

in this case, so equation (37) results in zero motion—i.e. a_{start} and a_{goal} are not $\mathcal{B}$-connected. In the language of sampling-based planning (Kavraki et al., 1996; Choset et al., 2005; LaValle, 2006), we say that a_{goal} is visible from a_{start} when using a straight-line local connection strategy in $\mathcal{A}$, but is not visible when using the analogous strategy in $\mathcal{B}$.

We can generalize this example as follows:

Lemma 6. *If $a, a' \in \mathcal{A}_{\text{stable}}$ are $\mathcal{B}$-connected and $a \neq a'$, then*

$$\Phi \circ \Psi|_{\mathcal{A}_{\text{stable}}}(a) \neq \Phi \circ \Psi|_{\mathcal{A}_{\text{stable}}}(a').$$

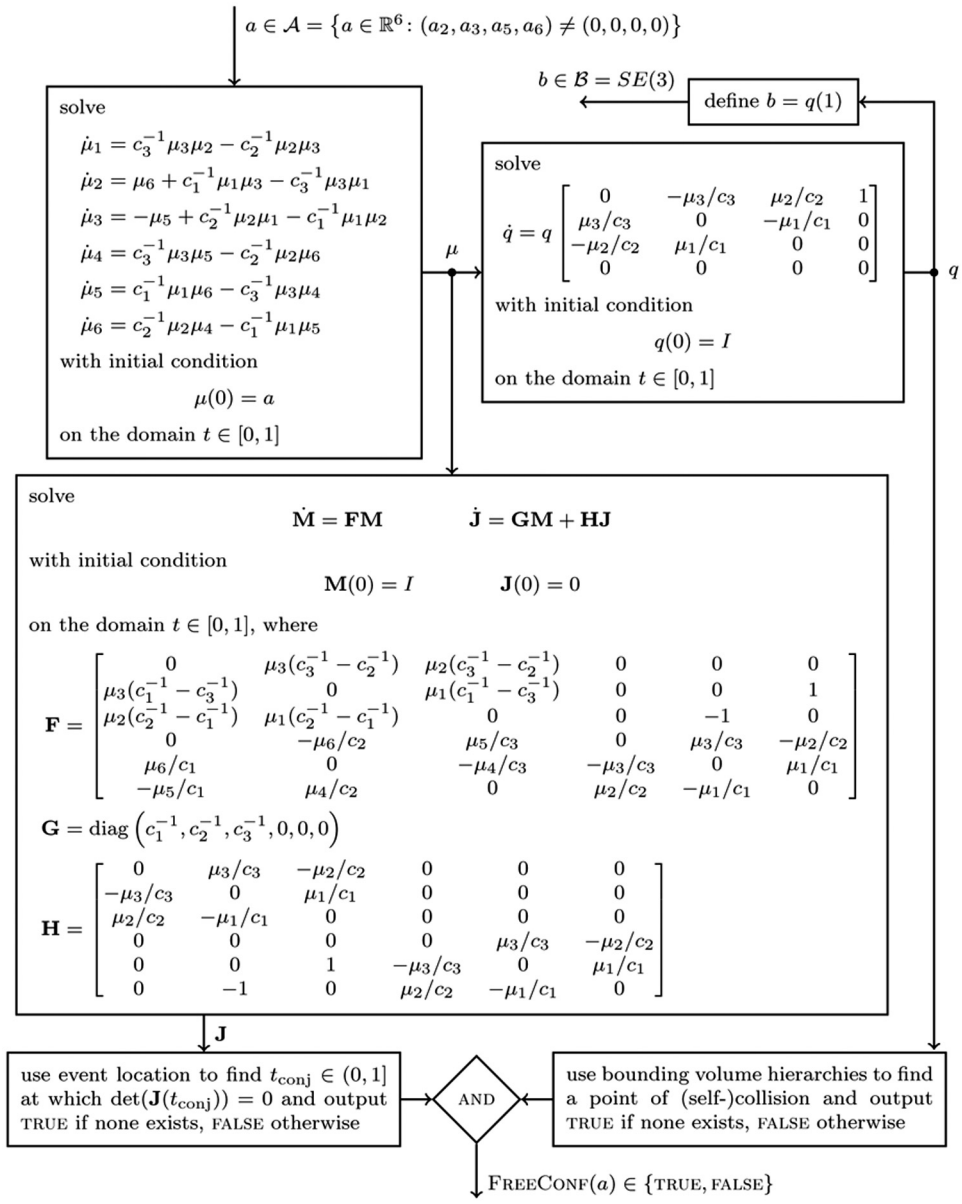

Fig. 6. Summary of computations required to check that a single configuration of the elastic rod, represented in coordinates by a point $a \in \mathcal{A} \subset \mathbb{R}^6$, is both stable and collision-free. We also produce the corresponding gripper placement $b \in \mathcal{B}$. The constants $c_1, c_2, c_3 > 0$ are assumed to be given.

Proof. Assume to the contrary that

$$b = \Phi \circ \Psi|_{\mathcal{A}_{\mathrm{stable}}}(a) = \Phi \circ \Psi|_{\mathcal{A}_{\mathrm{stable}}}(a') = b'.$$

Then, the straight-line path from b to b' results in zero motion, so we must have had $a = a'$, which is a contradiction. □

As a corollary, we can prove an even stronger result:

Lemma 7. *Let $a, a' a'' \in \mathcal{A}_{\mathrm{stable}}$. Assume that $a \neq a'$ and that*

$$\Phi \circ \Psi|_{\mathcal{A}_{\mathrm{stable}}}(a) = \Phi \circ \Psi|_{\mathcal{A}_{\mathrm{stable}}}(a').$$

If a and a'' are $\mathcal{B}$-connected, then a' and a'' are not $\mathcal{B}$-connected.

Proof. First, consider the case $a = a''$. We have $a' \neq a''$ by assumption, so Lemma 6 implies that a' and a'' are not $\mathcal{B}$-connected. Now, consider the case $a \neq a''$. Define $a_{\mathrm{start}} = a''$. Since $\Phi \circ \Psi|_{\mathcal{A}_{\mathrm{stable}}}(a) = \Phi \circ \Psi|_{\mathcal{A}_{\mathrm{stable}}}(a')$, the path $\alpha : [0,1] \to \mathcal{A}$ produced by equation (37) is the same regardless of whether $a_{\mathrm{goal}} = a$ or $a_{\mathrm{goal}} = a'$. In particular, since both $a \neq a'$ and $\alpha(1) = a$ by assumption, we must have $\alpha(1) \neq a'$. So, by definition, a' and a'' are not $\mathcal{B}$-connected. □

Lemma 7 implies that no fewer than three "straight-line paths" in $\mathcal{B}_{\mathrm{stable}}$ are required to connect two different equilibrium configurations that share the same boundary conditions. No such restriction exists on connections made

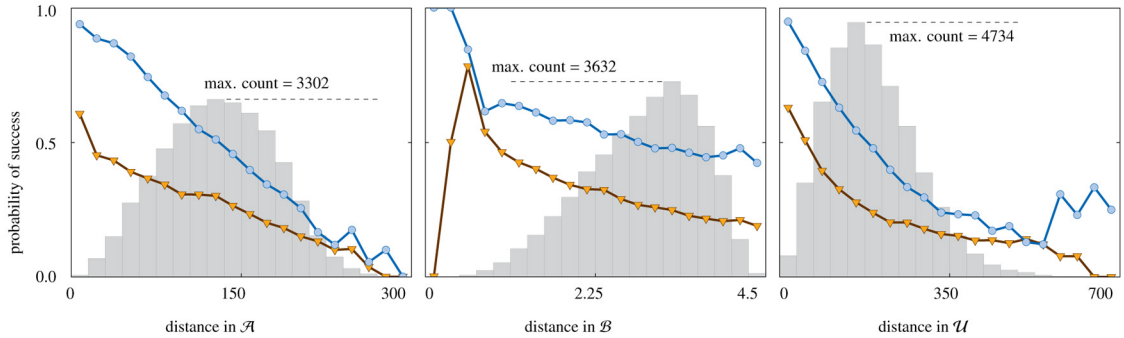

Fig. 7. Probability of successful local connection between randomly sampled points $a, a' \in \mathcal{A}_{\text{stable}}$ using straight-line paths in $\mathcal{A}$ (blue circles) and in $\mathcal{B}$ (orange triangles) as a function of distance measured in $\mathcal{A}$ (left), $\mathcal{B}$ (center), and $\mathcal{U}$ (right). A histogram shows the induced distribution after 30,000 samples over each measure of distance.

in $\mathcal{A}_{\text{stable}}$, strongly suggesting that $\mathcal{A}_{\text{stable}}$ has favorable visibility properties (in general) compared to $\mathcal{B}_{\text{stable}}$.

Figure 7 shows experimental results that support this claim. In each case, 30,000 pairs of points $a, a' \in \mathcal{A}_{\text{stable}}$ were generated by sampling uniformly at random in

$$\{a \in \mathcal{A}\colon\ |a_i| \leq 2\pi \text{ for } i = 1, 2, 3 \text{ and } |a_i| \leq 100 \text{ for } i = 4, 5, 6\}$$

and rejecting points that were not in $\mathcal{A}_{\text{stable}}$. We tested whether each pair of points was $\mathcal{A}$-connected and $\mathcal{B}$-connected (as in Section 5.5), including self-collision as well as stability constraints. We computed the probability that each type of connection was successful as a function of three distance measures:

- *Distance in $\mathcal{A}$:*

$$\sqrt{(a' - a)^T (a' - a)}.$$

- *Distance in $\mathcal{B}$:*

$$\sqrt{\theta^2 + v^T v},$$

where w, θ, and v are the exponential coordinates describing

$$b^{-1} b' = \left(\Phi \circ \Psi|_{\mathcal{A}_{\text{stable}}}(a)\right)^{-1} \left(\Phi \circ \Psi|_{\mathcal{A}_{\text{stable}}}(a')\right),$$

as defined in Section 5.5.

- *Distance in $\mathcal{U}$:*

$$\frac{1}{2} \int_0^1 \left(u' - u\right)^T \left(u' - u\right) \mathrm{d}t,$$

where $(q, u) = \Psi(a)$ and $(q', u') = \Psi(a')$ are as defined in Section 5.2.

Figure 7 shows that $\mathcal{A}$-connection was uniformly more likely to be successful as a function of distance than $\mathcal{B}$-connection. This result held for all three measures of distance (in $\mathcal{A}$, $\mathcal{B}$, and $\mathcal{U}$).

Figure 8 shows one more example of quasi-static manipulation to emphasize the consequences of this result. In this example, the rod moves through a sequence of six different equilibrium configurations that all share the same boundary conditions. In other words, each of the configurations shown in frames (a), (e), (i), (m), (q), and (u) is a different local optimum of equation (23) for the same gripper placement $b \in \mathcal{B}$. Remarkably, the motion between each consecutive pair of these local optima is a single straight-line path in $\mathcal{A}_{\text{stable}}$. So in total, the motion in Figure 8 can be represented by five straight-line paths in the chart that we derived. Lemma 7 implies that—at minimum—fifteen straight-line paths in $\mathcal{B}_{\text{stable}}$ would have been required to move through this same sequence of equilibrium configurations. The empirical results in Figure 7 suggest that even more would likely have been required.

Video of the examples in Figures 1 and 8 are included in Extension 1.

7. Conclusion

Our contribution in this paper was to show that the set of equilibrium configurations for a Kirchhoff elastic rod held by a robotic gripper is a smooth manifold of finite dimension that can be parameterized by a single (global) coordinate chart. The fact that we ended up with a finite-dimensional smooth manifold is something that might have been guessed in hindsight (its dimension—six—is intuitive given that the gripper moves in $SE(3)$), but the fact that this manifold admitted a global chart is something that we find remarkable. Our results led to a simple algorithm for manipulation planning, which at the outset had seemed very hard to solve.

Although we call our algorithm "simple", an efficient implementation of this algorithm requires consideration of certain details that remain to be addressed. For example, to verify static equilibrium, Theorem 7 (also see Figure 6) requires a check that $\det(\mathbf{J}(t))$ does not vanish on $(0, 1]$. Currently, we approximate this check by using a method of event location in ordinary differential equations, as described by Shampine and Thompson (2000) and implemented by `ode45` in MATLAB. We could also have

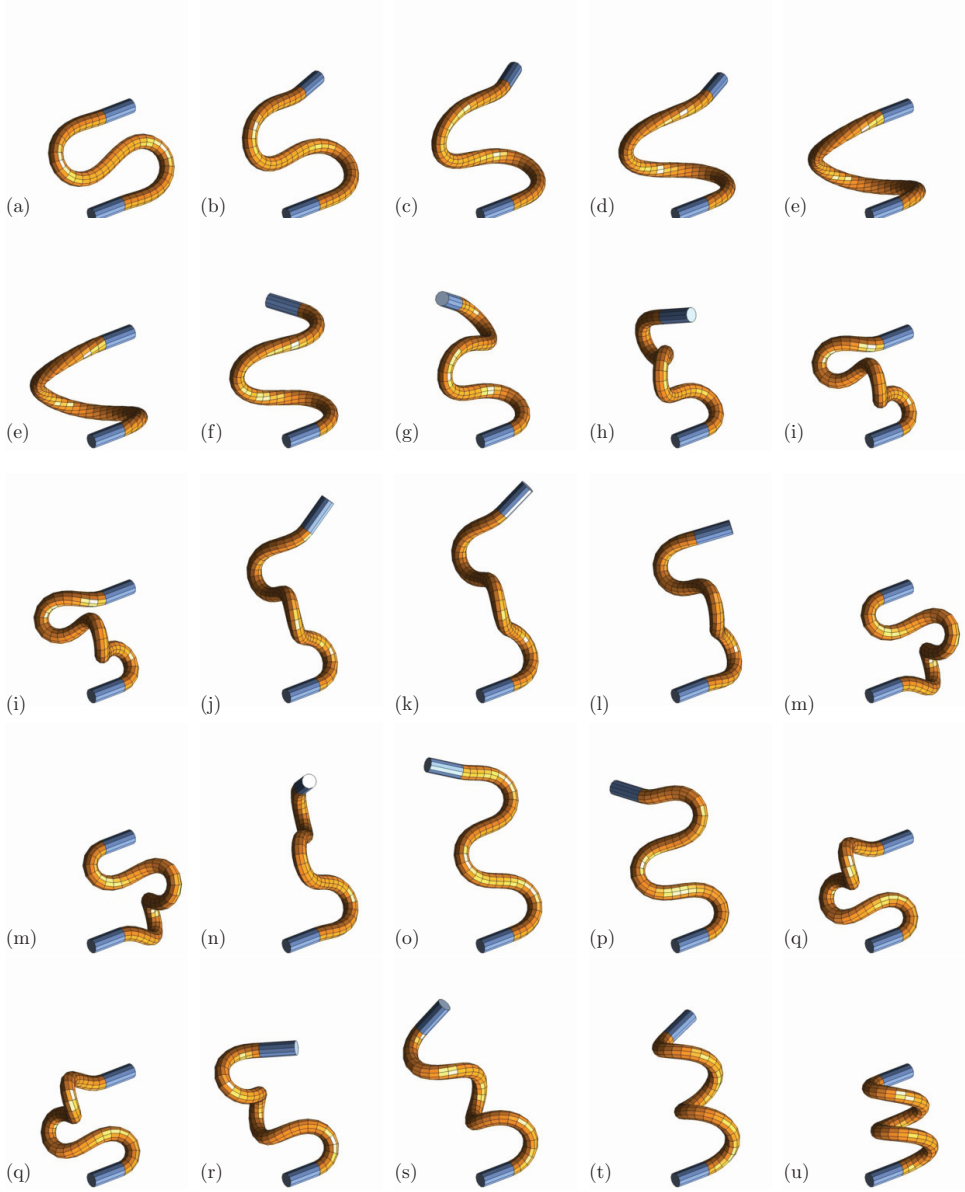

Fig. 8. Another example of quasi-static manipulation by robotic grippers (blue) of an elastic rod (orange), in which we are exploring a zoo of equilibrium configurations—shown in frames (a), (e), (i), (m), (q), and (u)—that all share the same boundary conditions. Remarkably, each row corresponds to a straight-line path in the global coordinate chart $\mathcal{A}$ that we derived.

approximated this check by sampling t at some fixed resolution. Neither approach is guaranteed to produce a correct result, and both approaches suffer from the classic tradeoff between resolution (hence, computation time) and accuracy. We would much prefer to implement an adaptive or "exact" approach, as suggested—for example—by Schwarzer et al. (2005). Doing so is problematic, however, since $\det(\mathbf{J}(t))$ and all its derivatives vanish at $t = 0$. Along similar lines, the computation of both $\mathbf{J}$ and q requires the integration of linear, time-varying, matrix differential equations. Again, we have done so simply by using `ode45` in MATLAB, with a sufficiently low error tolerance. Ignoring the obvious structure in equations (25) and (33) makes our current implementation highly inefficient. The use of variational integrators (West, 2004) would be a straightforward way to improve performance.

There are several other opportunities for future work. First, the coordinates we derive can be interpreted as forces and torques at the base of the elastic rod, so $\mathcal{A}$ is exactly the space over which to perform inference in state estimation with a force/torque sensor. Second, our model of an elastic rod depends on three physical parameters $c_1, c_2, c_3 > 0$. Finding these parameters from observations of equilibrium configurations can be cast as an inverse optimal control problem (Javdani et al., 2011). The structure established by Theorem 6 allows us to define a notion of orthogonal distance between $\mathcal{C}$ and these observations, similar to Keshavarz et al. (2011), and may lead to an efficient method

of solution. Third, we note that an elastic inextensible strip (or "ribbon") is a developable surface whose shape can be reconstructed from its centerline (Starostin and van der Heijden, 2008). This centerline conforms to a similar model as the elastic rod and is likely amenable to similar analysis, which may generalize to models of other developable surfaces. Finally, it may be possible to generalize our approach to deal with other applied forces. The consideration of gravity—as the gradient of a potential—should be straightforward, although it complicates our approach to Lie–Poisson reduction. The consideration of other forces arising from interaction between different parts of the elastic rod (e.g. self-collision) is apparently much harder.

Acknowledgements

The authors would like to thank Don Shimamoto for his many helpful comments, in particular those leading to the current proof of Lemma 4. Thanks also to the organizers, anonymous reviewers, and audience at WAFR 2012, whose suggestions helped to improve this paper.

Funding

This work was supported by the National Science Foundation (grant numbers CPS-0931871 and CMMI-0956362).

Notes

1. This model is slightly different from the one we describe in Section 5—for a discussion of the relationship between these two models, see Biggs et al. (2007).
2. The *smooth topology* is also called the C^∞ topology and the Whitney topology in the literature (Hirsch, 1976).

References

Agarwal P, Guibas L, Nguyen A, Russel D and Zhang L (2004) Collision detection for deforming necklaces. *Computational Geometry* 28(2–3): 137–163.

Agrachev AA and Sachkov YL (2004) *Control Theory from the Geometric Viewpoint*. Berlin: Springer.

Amato NM and Song G (2002) Using motion planning to study protein folding pathways. *Journal of Computational Biology* 9 (2): 149–168.

Antman SS (2005) *Nonlinear Problems of Elasticity*. New York: Springer.

Asano Y, Wakamatsu H, Morinaga E, Arai E and Hirai S (2010) Deformation path planning for manipulation of flexible circuit boards. In: *IEEE/RSJ international conference on intelligent robots and systems (IROS '10)*, Taipei, Taiwan, 18–22 October 2010, pp. 5386–5391. Piscataway: IEEE Press.

Balkcom DJ and Mason MT (2008) Robotic origami folding. *International Journal of Robotics Research* 27(5): 613–627.

Bell M and Balkcom D (2008) Knot tying with single piece fixtures. In: *IEEE international conference on robotics and automation (ICRA '08)*, Pasadena, CA, 19–23 May 2008, pp. 379–384. Piscataway: IEEE Press.

Bergou M, Wardetzky M, Robinson S, Audoly B and Grinspun E (2008) Discrete elastic rods. *ACM Transactions on Graphics* 27 (3): 1–12.

Biggs J, Holderbaum W and Jurdjevic V (2007) Singularities of optimal control problems on some 6-D Lie groups. *IEEE Transactions on Automation and Control* 52(6): 1027–1038.

Bloch A, Krishnaprasad P, Marsden J and Ratiu T (1996) The Euler–Poincaré equations and double bracket dissipation. *Communications in Mathematical Physics* 175(1): 1–42.

Bretl T and McCarthy Z (2012) Equilibrium configurations of a Kirchhoff elastic rod under quasi-static manipulation. In: *10th international workshop on the algorithmic foundations of robotics (WAFR '12)*, Cambridge, USA, 13–15 June 2012.

Camarillo DB, Milne CF, Carlson CR, Zinn MR and Salisbury JK (2008) Mechanics modeling of tendon-driven continuum manipulators. *IEEE Transactions on Robotics* 24(6): 1262–1273.

Chirikjian GS and Burdick JW (1995) The kinematics of hyper-redundant robot locomotion. *IEEE Transactions on Robotics and Automation* 11(6): 781–793.

Choset H, Lynch K, Hutchinson S, Kanto G, Burgard W, Kavraki L et al. *Principles of Robot Motion: Theory, Algorithms, and Implementations*. Cambridge: MIT Press.

Clements TN and Rahn CD (2006) Three-dimensional contact imaging with an actuated whisker. *IEEE Transactions on Robotics* 22(4): 844–848.

Gopalakrishnan K and Goldberg K (2005) D-Space and deform closure grasps of deformable parts. *International Journal of Robotics Research* 24(11): 899–910.

Gottschalk S, Lin M and Manocha D (1996) OBB-tree: A hierarchical structure for rapid interference detection. *Computational Graphics* 30: 171–180.

Henderson ME and Neukirch S (2004) Classification of the spatial equilibria of the clamped elastica: Numerical continuation of the solution set. *International Journal of Bifurcation & Chaos in Applied Sciences & Engineering* 14(4): 1223–1239.

Hirsch MW (1976) *Differential Topology*. Berlin: Springer-Verlag, pp. 34–35.

Hoffman KA (2004) Methods for determining stability in continuum elastic-rod models of DNA. *Philosophical Transactions of the Royal Society of London. Series A: Mathematical, Physical and Engineering Sciences* 362(1820): 1301–1315.

Hopcroft JE, Kearney JK and Krafft DB (1991) A case study of flexible object manipulation. *International Journal of Robotics Research* 10(1): 41–50.

Inaba M. Hand eye coordination in rope handling. *J. of Robotics Society Japan*, 3(6): 32–41, 1985.

Ivey TA and Singer DA (1999) Knot types, homotopies and stability of closed elastic rods. *Proceedings of the London Mathematical Society* 79(2): 429–450.

Jansen R, Hauser K, Chentanez N, van der Stappen F and Goldberg K (2009) Surgical retraction of non-uniform deformable layers of tissue: 2D robot grasping and path planning. In: *IEEE/RSJ international conference on intelligent robots and systems (IROS '09)*, St. Louis, MO., 10–15 October 2009, pp. 4092–4097. Piscataway: IEEE Press.

Javdani S, Tandon S, Tang J, O'Brien JF and Abbeel P (2011) Modeling and perception of deformable one-dimensional objects. In: *IEEE international conference on robotics and automation (ICRA '11)*, Shanghai, China, 9–13 May 2011, pp. 1607–1614. Piscataway: IEEE Press.

Jurdjevic V (2005) *Integrable Hamiltonian Systems on Complex Lie Groups*. Providence: American Mathematical Society.

Kavraki LE, Svetska P, Latombe J-C and Overmars M (1996) Probabilistic roadmaps for path planning in high-dimensional configuration spaces. *IEEE Transactions on Robotics and Automation* 12(4): 566–580.

Keshavarz A, Wang Y and Boyd S (2011) Imputing a convex objective function. In: *IEEE multi-conference on systems and control*, Denver, CO., 28–30 September 2011, pp. 613–619. Piscataway: IEEE Press.

Lamiraux F and Kavraki LE (2001) Planning paths for elastic objects under manipulation constraints. *International Journal of Robotics Research* 20(3): 188–208.

Langer J and Singer D (1984) The total squared curvature of closed curves. *Journal of Differential Geometry* 20: 1–22.

Langer J and Singer DA (1996) Lagrangian aspects of the Kirchhoff elastic rod. *SIAM Review* 38(4): 605–618.

Latombe JC (1991) *Robot Motion Planning*. Boston: Kluwer Academic Publishers.

LaValle SM (2006) *Planning Algorithms*. New York: Cambridge University Press.

Lee JM (2003) *Introduction to Smooth Manifolds*. New York: Springer.

Lin Q, Burdick J and Rimon E (2000) A stiffness-based quality measure for compliant grasps and fixtures. *IEEE Transactions on Robotics and Automation* 16(6): 675–688.

Marsden JE and Ratiu TS (1999) *Introduction to Mechanics and Symmetry: A Basic Exposition of Classical Mechanical Systems*. New York: Springer.

McCarthy Z and Bretl T (2012) Mechanics and manipulation of planar elastic kinematic chains. In: *IEEE international conference on robotics and automation (ICRA '12)*, St. Paul, USA, 14–18 May 2012, pp. 2798–2805. Piscataway: IEEE Press.

Moll M and Kavraki LE (2006) Path planning for deformable linear objects. *IEEE Transactions on Robotics* 22 (4): 625–636.

Murray R, Li ZX and Sastry S (1994) *A Mathematical Introduction to Robotic Manipulation*. Boca Raton: CRC Press.

Neukirch S and Henderson M (2002) Classification of the spatial equilibria of the clamped elastica: Symmetries and zoology of solutions. *Journal of Elasticity* 68(1): 95–121.

Pontryagin LS, Boltyanskii VG, Gamkrelidze RV and Mishchenko EF (1962) *The Mathematical Theory of Optimal Processes*. New York: Wiley.

Rucker DC, Webster RJ, Chirikjian GS and Cowan NJ (2010) Equilibrium conformations of concentric-tube continuum robots. *International Journal of Robotics Research* 29 (10): 1263–1280

Sachkov Y (2008a) Conjugate points in the Euler elastic problem. *Journal of Dynamical and Control Systems* 14 (3): 409–439.

Sachkov Y (2008b) Maxwell strata in the Euler elastic problem. *Journal of Dynamical and Control Systems* 14(2): 169–234.

Saha M and Isto P (2007) Manipulation planning for deformable linear objects. *IEEE Transactions on Robotics* 23(6): 1141–1150.

Sánchez G and Latombe J-C (2002) On delaying collision checking in PRM planning: Application to multi-robot coordination. *International Journal of Robotics Research* 21(1): 5–26.

Schwarzer F, Saha M and Latombe JC (2005) Adaptive dynamic collision checking for single and multiple articulated robots in complex environments. *IEEE Transactions on Robotics* 21 (3): 338–353.

Shampine L and Thompson S (2000) Event location for ordinary differential equations. *Computers & Mathematics with Applications* 39(5–6): 43–54.

Shi Y and Hearst JE (1994) The Kirchhoff elastic rod, the nonlinear Schrödinger equation, and DNA supercoiling. *Journal of Chemical Physics* 101(6): 5186–5200.

Shi Y, Hearst JE, Bishop TC and Halvorson HR (1998) Erratum: "the Kirchhoff elastic rod, the nonlinear Schrödinger equation, and DNA supercoiling" [J. Chem. Phys. 101, 5186 (1994)]. *Journal of Chemical Physics* 109(7): 2959–2961.

Solomon JH and Hartmann MJZ (2010) Extracting object contours with the sweep of a robotic whisker using torque information. *International Journal of Robotics Research* 29 (9): 1233–1245.

Souéres P and Boissonnat J (1998) Optimal trajectories for nonholonomic mobile robots. In: Laumond J-P (ed) *Robot Motion Planning and Control*. Berlin: Springer, vol. 229, ch. 3, pp. 93–170.

Starostin EL and van der Heijden GHM (2008) Tension-induced multistability in inextensible helical ribbons. *Physical Review Letters* 101(8): 084301.

Takamatsu J, Morita T, Ogawara K, Kimura H and Ikeuchi K (2006) Representation for knot-tying tasks. *IEEE Transactions on Robotics* 22(1): 65–78.

Tanner H (2006) Mobile manipulation of flexible objects under deformation constraints. *IEEE Transactions on Robotics* 22 (1): 179–184.

van den Berg J, Miller S, Goldberg K and Abbeel P (2011) Gravity-based robotic cloth folding. Algorithmic Foundations of Robotics IX Springer Tracts in Advanced Robotics Volume 68, 2011, pp 409–424 Editors: Hsu, David; Isler, Volkan; Latombe, Jean-Claude; Lin, Ming C. http://dx.doi.org/10.1007/978-3-642-17452-0_24 Springer Berlin Heidelberg

Wakamatsu H, Arai E and Hirai S (2006) Knotting/unknotting manipulation of deformable linear objects. *International Journal of Robotics Research* 25(4): 371–395.

Walsh G, Montgomery R and Sastry S (1994) Optimal path planning on matrix Lie groups. In: *IEEE conference on decision and control*, Lake Buena Vista, FL., 14–16 December 1994, vol. 2, pp. 1258–1263. Piscataway: IEEE Press.

Webster RJ and Jones BA (2010) Design and kinematic modeling of constant curvature continuum robots: A review. *International Journal of Robotics Research* 29(13): 1661–1683

West M (2004) *Variational integrators*. PhD Thesis, California Institute of Technology, USA.

Yamakawa Y, Namiki A and Ishikawa M (2011) Motion planning for dynamic folding of a cloth with two high-speed robot hands and two high-speed sliders. In: *IEEE international conference on robotics and automation (ICRA '11)*, Shanghai, China, 9–13 May 2011, pp. 5486–5491. Piscataway: IEEE Press.

Appendix: Index to Multimedia Extensions

The multimedia extension page is found at www.ijrr.org

Table of Multimedia Extensions

Extension	Media Type	Description
1	Video	Five examples of quasi-static manipulation. This video shows five examples of quasistatic manipulation. The first three examples should clarify the difference between a "straight-line path" in the space of boundary conditions and in the global coordinate chart that we derive in the paper. The last two examples correspond to Figures 1 and 8 in the paper.